Murray *et al. Applied Biological Chemistry* (2024) 67:28
https://doi.org/10.1186/s13765-024-00876-9

KSABC
The Korean Society for Applied Biological Chemistry

ARTICLE

Open Access

Exploring the binding interactions of NOP receptor with designed natural phytochemical-neuropeptide conjugates: an in silico and SPR study

Molly E. Murray[1], Beatriz G. Goncalves[1], Mary A. Biggs[1], Sophia A. Frantzeskos[1], Charlotta G. Lebedenko[1] and Ipsita A. Banerjee[1*]

Abstract

The Nociceptin/orphanin FQ peptide (NOP) receptor is considered a member of the opioid receptor subfamily of G-protein coupled receptors (GPCRs) which has been shown to be present in many parts of the central nervous system (CNS). It plays biologically diverse roles in pain modulation, immune response and in neurodegenerative diseases. In this work, phytochemical conjugates of two known neuropeptides, melanocyte inhibition factor (MiF-1) and mammalian amidated neuropeptide NPFF with pain modulating ability were developed. The binding interactions of those conjugates with NOP receptor was examined as an approach to develop novel natural compounds that can modulate NOP receptor activity. The selected phytochemicals are well-known for their antioxidant abilities and are derived either from natural alkaloids (betanin), polyphenols (gallic acid and sinapic acid) or terpenes (pomolic acid). Each of the phytochemicals selected are antioxidants which may play a role in mitigating diseases. Three conjugates of betanin were designed with each peptide by conjugating each of the three carboxylic acid groups of betanin with the peptides, while all others were mono-conjugates. Our results indicated that the betanin conjugates with both peptides showed strong binding interactions while the pomolate-peptide conjugates showed moderate binding. In general, NPFF and its conjugates showed stronger binding with the receptor. Docking and molecular dynamics studies revealed that binding interactions occurred at the binding pocket encompassing the transmembrane helices TM1, TM3 and TM7 in most cases, with the ligands binding deep within the hydrophobic core. The binding interactions were further confirmed experimentally through SPR analysis, which also showed higher binding with the betanin conjugates. MMGBSA studies indicated that the binding energies of MiF-1 conjugates were higher compared to neat MiF-1. However, in the case of NPFF, while the betanin conjugates showed enhancement, in some cases the binding energies were found to be slightly reduced compared to neat NPFF. Overall our studies reveal that such natural phytochemical derivatives that can bind to the NOP receptor when conjugated to the mammalian amidated neuropeptide NPFF and the short sequence of melanocyte inhibiting factor MiF-1 may be potentially developed for further laboratory studies for potential pharmaceutical applications.

Keywords Nociceptin/orphanin FQ peptide receptor (NOP) receptor, Peptide binding, Melanocyte inhibiting factor-1, Molecular dynamics

*Correspondence:
Ipsita A. Banerjee
banerjee@fordham.edu
Full list of author information is available at the end of the article

Introduction

The nociceptin receptor (NOPR) was considered to be a part of the opioid receptor family [1] of G-protein coupled receptors (GPCRs) (Mu, Delta and Kappa) though over the years several studies have suggested both resemblance and dissimilarities of the NOPR with other opioid receptors [2, 3]. The neuropeptide nociceptin/orphanin FQ (N/OFQ) is a 17 amino-acid (FGGFTGARKSARKLANQ) peptide which has been reported to be its endogenous ligand that binds with high affinity and specificity to the NOP receptor [4] resulting in the inhibition of adenylate cyclase, with increased K^+ conductance and reduction in Ca^{+2} conductance. The N/OFQ–NOP system is expressed in the brain, spinal cord and dorsal root ganglia. In the brain, it is found in various regions including the hypothalamus, cingulate, periaqueductal gray (PAG), amygdala, locus ceruleus (LC), endopiriform nucleus, raphe nuclei, hippocampus, ventral tegmental area (VTA), [5] in cortical and subcortical motor areas, and also in dopaminergic neurons of the substantia nigra compacta [6]. Typically, the peptide N/OFQ functions as an inhibitory neurotransmitter, acting via the NOP receptor to suppress cellular neuronal activity and release of other neurotransmitters, and provides a counterbalance to excitatory systems to maintain homeostasis [7]. However, changes to the NOP-N/OFQ system have been shown to be implicated in diseased states, making it a potential therapeutic target. In particular, it has been reported that dysregulation of NOP-N/OFQ occurs in Parkinson's disease (PD), where its activity is upregulated [8]. Other reports have also suggested its upregulation in chronic pain and depression [9]. Additionally, it has been suggested that NOP-N/OFQ receptor plays a modulatory role in immune system functions [10]. In a pioneering study, Watson and co-workers reported an increase in pre-pro N/OFQ amounts with a concomitant decrease in the mRNA levels of NOP in the substantia nigra compacta (SNc) portion of the brain of PD diseased rat models [11]. Furthermore, N/OFQ levels have been found to be elevated in the cerebrospinal fluid of Parkinson's patients, [12] implicating N/OFQ upregulation in the pathophysiology of Parkinson's disease in humans. In a separate study, it was revealed that both NOP receptor protein and N/OFQ immunoreactivity were increased in rats with inflammatory pain [13]. Thus, several NOP receptor antagonists are being developed. In a recent study conducted by Borruto and co-workers, NOP receptor antagonists such as LY2817412 showed reduction in alcohol-seeking behavior and prevented alcoholism relapse in mice [14]. In another study, the NOP receptor antagonist drug LY2940094 was found to alleviate depression symptoms found in patients suffering from major depressive disorder [15]. Another NOP receptor agonist, 1-[(3R,4R)-1-cyclooctylmethyl-3-hydroxymethyl-4-piperidyl]-3-ethyl-1,3-dihydro-2H benzimidazol-2-one (J-113397), was shown to reduce parkinsonian symptoms in rats when co-administered with Levodopa (L-DOPA) [16]. NOP receptor agonists have also been known to reduce the reward effects of drug abuse medications and opiates [17]. These findings support the need for developing NOP receptor modulators that may impact several biological processes and potentially mitigate Parkinson's disease.

It is well-known that even though the NOP receptor structure shows a substantial homology with the other opioid receptors, it does not have a high affinity toward other opioid ligands. For example, ligands such as oliceridine [18], which is a biased opioid ligand for the mu receptor or HS665, which is highly selective toward the kappa receptor, did not show binding with the NOP receptor [19]. In fact, the NOP receptor has been shown to have an unique mechanism of activation compared to the opioid receptors mu, delta and kappa. In a study conducted by Daga and co-workers, [20] the first active-state homology model of the NOP receptor was examined through molecular dynamics simulations. The study revealed that NOP activation involved movements of transmembrane helices 3 and 6 and several other activation microswitches consistent with GPCR activation. Specifically, it was shown that the shortest active fragment of endogenous agonist peptide nociceptin/orphanin FQ (residues 1–13) showed interactions between the extracellular loop 2 region (EL2) and the positively charged residues, arginine and lysine, in the (8–13) region of the N/OFQ peptide. Thus, polar interactions with residues at the extracellular end of the transmembrane domain and EL2 loop led to ligand-induced re-organization of polar regions during receptor activation. Other non-peptidic small-molecule NOP receptor ligands such as spiropiperidine and Ro 64–6198 have also been docked into the NOP homology model constructed based on the Palczewki bovine rhodopsin crystal structure [21] and the beta2-adrenergic receptor [22]. These agonists were also shown to bind to the transmembrane binding pocket region and interactions with the same receptor residues as the N-terminus residues of the N/OFQ peptide were found; though, little interaction was observed with the EL2 loop region in those models.

To further investigate the binding interactions with the NOP receptor and design new potential drug candidates that can modulate receptor binding, in this work, we designed phytochemical-peptide conjugates to explore the binding interactions. Specifically, we utilized two peptides as our starting point. The peptide Melanocyte Inhibiting Factor-1 peptide (MiF-1) [Pro-Leu-Gly-NH_2] which is a fragment of the hormone oxytocin and has been shown to modify motor activity response by modulating dopamine

receptors D2 and D4 activity [23, 24]; and another short peptide, Neuropeptide FF (NPFF) [FLFQPQRFa], which is a known pain modulating peptide that has shown anti-opioid effects upon chronic administration of opioid agonists [25]. This peptide also has a N-terminal phenylalanine motif like the endogenous N/OFQ peptide and the C-terminal amide also imparts a constrained structure. To our knowledge, this is the first study where the binding interactions of these peptides have been explored with the NOP receptor. We further designed plant alkaloid, terpene, and polyphenol conjugates of these peptides to enhance hydrophobic interactions as well as render anti-oxidant, anti-nociceptive and anti-inflammatory properties. In previous studies, several polyphenols have been explored as drug candidates against Parkinson's Disease [26]. Furthermore, flavonoids have been shown to have a binding affinity toward opioid receptors [27]. The plant derived Triphala which is rich in polyphenols such as gallic acid, ellagic acid, chebulic acid, and contains several flavonoids, has been shown to be a target that can potentially bind to the NOP receptor [28]. Cyclic analogues of N/OFQ peptide with constrained structures have been designed and have been shown to have enhanced binding interactions with the NOP receptor [29]. In addition, several peptides and peptide derivatives have been developed to modulate NOP receptor activity. Some examples include [Nphe1] N/OFQ (1–13) NH_2 [30]; [$Nphe^1$, Arg^{14}, Lys^{15}] N/OFQ-NH_2 (UFP-101) [31]; and [(pF)$Phe^4$$Aib^7$$Arg^{14}$$Lys^{15}$] N/OFQ-$NH_2$ (UFP-112) [32] which contained specific modifications of the N/OFQ peptide. Additionally, Guerrini and co-workers utilized a peptide wilding approach (PWT), to develop three tetra-branched derivatives of N/OFQ, PWT1-N/OFQ, PWT2-N/OFQ, and PWT3-N/OFQ which were found to act as potent NOP agonists [33]. In another study Lohman and co-workers developed helix constrained peptides where two lysine and two aspartic acid residues were incorporated into the C-terminus of the nociceptin peptide and cross-linked. The peptides were found to be potent agonists and antagonists of NOPR [34].

While there are several similarities between the mu, delta and kappa receptors, NOPR is conformationally different from other opioid receptors [35, 36]. It is well-known that the endogenous ligand N/OFQ, activates NOP by interacting with residues at and around its B chain residues Asp130, Lys201, Trp276, Val279, Gln286, and Arg302 [20]. These findings have also been consistent across other NOP agonists, including its native ligand nociceptin and several of its derivatives [37, 38].

Herein, we have designed ten novel peptide conjugates by conjugating four natural anti-inflammatory, antioxidant phytochemicals (sinapic acid; gallic acid, betanin and pomolic acid) with MiF-1 and NPFF and explored their ability to bind to the NOP receptor. We also compared the binding interactions with neat MiF-1 and NPFF with both receptors. Among the phytochemicals, betanin is an anti-inflammatory compound derived from beetroot and is found to decrease hypersensitivity with regard to neuropathic pain, and is currently being investigated for many therapeutic interventions [39]. Betanin has three free carboxylic groups, therefore three conjugates (mono, di- and tri- conjugates) were designed with each peptide by conjugating the N-terminal of the peptide with each of the carboxyl groups of betanin. Gallic acid is found in numerous foods such as berries, grapes, and walnuts and has been shown to reduce neuropathic pain, distinguishing it as a potential antinociceptive compound [40]. Pomolic acid is a triterpene with numerous medicinal properties and has been shown to reduce oedema in mice [41]. Sinapic acid is a multifaceted antioxidant polyphenol with potential therapeutic effects on cancers, neurodegeneration, inflammation, and infection [42]. More recently, sinapic acid (SA) has been shown to reduce the progression of streptozotocin induced Type II diabetic neuropathy [43]. All of the above phytochemical derivatives contain hydrophobic moieties. In previous work, hydrophobic scaffolds such as spiro-isoquinolines, [44] triazaspirodecanone [45], and phenyl piperidines [46] have been found to bind to the NOP receptor efficiently. Thus, we hypothesized that the hydrophobic moieties of the compounds selected may also potentially enhance affinity toward the NOPR upon conjugation with MiF-1 or NPFF peptide. The chemical structures of the peptides and the designed conjugates utilized in this study are shown in Fig. 1.

We first conducted a computational investigation in order to explore the interactions of the conjugates and the peptides with NOPR using docking studies and molecular dynamics simulations. While most conjugates were found to bind to the transmembrane helices 2, 3 and 7 primarily through hydrophobic interactions and hydrogen bonding, in some cases interactions were also seen with the Cys200 residue of the EL2 loop. As a proof of concept, we also determined the binding interactions of the optimal conjugates with NOPR experimentally using surface plasmon resonance (SPR) analysis. Our results indicated that the binding was found to be concentration dependent, and that the betanin conjugates were found to have the highest binding with the NOP receptor with both peptides, while gallate-MiF-1 displayed higher binding amongst the MiF-1 conjugates. Overall, this study for the first time explores the binding interactions of naturally derived phytochemicals conjugated with neuropeptides MiF-1 and NPFF. The betanin, pomolate, and gallate-conjugates may potentially be developed for modulating NOP receptor binding and for drug design. Further laboratory studies into their

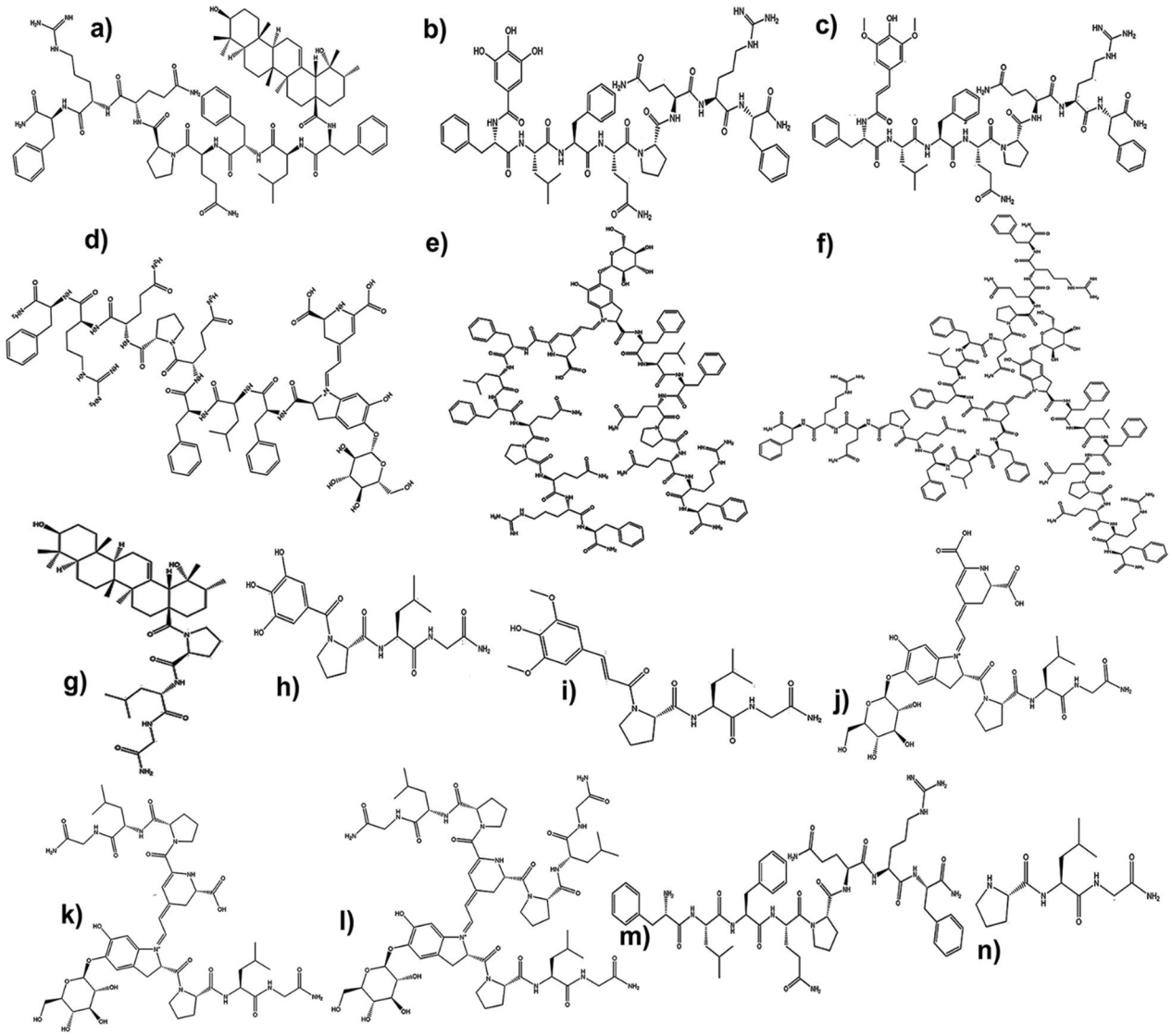

Fig. 1 Chemical structures of peptides and conjugates designed in this study. **a**–**f** NPFF conjugated to (**a**) pomolate; (**b**) gallate; (**c**) sinpate; (**d**) Betanin-monoconjugate; (**e**) Betanin-di-conjugate; (**f**) Betanin-tri-conjugate with NPFF. **g**–**l** MiF-1 conjugated to (**g**) pomolate; (**h**) gallate; (**i**) sinapate; (**j**) Betanin-monoconjugate; (**k**) Betanin-di-conjugate; (**l**) Betanin-tri-conjugate with MiF-1. (**m**) NPFF; (**n**) MiF-1

agonistic or antagonistic activity can provide insights into their development as pharmacological candidates for potential medicinal applications.

Methods

Computational methods

Conjugate design

The software ChemDraw 20.1.1 was used to design the 2D structures of each molecule to be studied including the peptides MiF-1 and NPFF. In general, the free carboxylic acid groups of the polyphenols were conjugated with the free amine groups of the peptides. For betanin, 6 conjugates were created, due to the presence of three carboxyl groups. Thus, Betanin-MiF-1, Betanin-di-MiF-1 and Betanin-tri-MiF-1 were created. Similarly, three conjugates of betanin-NPFF were created. The 2D structures were then exported to ChemDraw 3D (Perkin Elmer Chem Office 2020 -Version 20.0) for geometry optimization and MM2 energy minimization, and then saved as .pdb files and visualized on PyMOL.

Sigma profiles (COSMOtherm)

The molecular surface charge density of each of the peptides and peptide-based conjugates were investigated using the Conductor-like Screening Model for Real Solvents (COSMO-RS). Sigma profiles and sigma surfaces

for the compounds were generated with the software Turbomole and Cosmotherm (2020) [47]. Sigma profiles are calculated using density functional theory to determine the probability of the molecular surface charge [48]. Hydrogen bond donors are indicated in the region lower than -0.0082 e/Å^2 while hydrogen bond acceptors fall into the region greater than + 0.0082 e/Å^2. The nonpolar region is exhibited in the range between -0.0082 e/Å^2 and + 0.0082 e/Å^2 [49]. Data for sigma profiles was exported into Excel for analysis.

Surface cavities (POCASA)

To determine binding pockets of the Nociceptin/Orphanin FQ Peptide Receptor (PDB ID: 4EA3) [50], we used the webserver POCASA [51] which utilizes a spherical probe to scan the surface of the protein. Any pockets or cavities that are detected are then ranked based on Volume-Depth (VD). A probe radius of 2 Å, single point flag of 16, protein depth flag of 18, and grid size of 1 Å were set as parameters for the sphere, and results were visualized using PyMOL.

Docking studies

The binding interactions between each peptide and conjugate with NOPR was evaluated with the molecular docking software AutoDock Vina 1.1.2. This software employs gradient optimization to determine the strongest binding affinities for each ligand-receptor pairing [52]. Receptors and ligands were initially prepared using AutoDockTools-1.5.6. First, any attached ligands were removed from the receptor using PyMOL. Then, polar hydrogens and kollman charges were added, and the structures were saved as .pdbqt files. The peptide conjugate ligands were then prepared by selection for Autodock 4, and then combined with each receptor to produce a specific grid box of coordinates signifying the anticipated binding site. This process was repeated for each receptor and ligand pairing. The highest binding affinity was indicated by the lowest RMSD value for each output being recorded. The results of the docked receptor-ligands were then visualized using PyMOL [53].

Receptor-ligand interactions (PLIP)

The results obtained from docking studies containing the most optimal receptor-ligand poses were uploaded to the Protein–Ligand Interaction Profiler (PLIP) webserver. PLIP allows for visualization of binding interactions with the residues within the binding pocket [54]. Results were visualized on PyMOL and various interactions obtained were tabulated.

Molecular dynamics

Molecular dynamics simulations were evaluated using the software Desmond 2021–3 [55]. In order to prepare each receptor-ligand complex, first within PyMOL, hydrogens were added to the optimal binding affinity pose obtained from each Autodock run, and the structure was exported as a .mae file. This file was opened in the software Maestro. Protein Preparation Wizard was used to prepare the receptor. Epik was used at pH 7.0 ± 2.0 to assign bond orders, generate het states, and add hydrogens to the receptor, and then the system was preprocessed and optimized at PROPKA pH of 7.0. This prepared receptor was then combined with the ligand, and the system was assembled using System Builder with the SPC solvent model. This process created an orthorhombic box size through Maestro's buffer method, which was then minimized in order to properly encompass the entire structure. The system was next neutralized with Cl^- counter ions. The OPLS_2005 forcefield was used to run the atomistic molecular dynamics simulations. The system was equilibrated, first with the Brownian Dynamics NVT simulation at a temperature of 10 K, with small timesteps and restraints on solute heavy atoms for 100 ps. The next portion of the NVT simulation at 10 K with small timesteps and restraints on solute heavy atoms was run for 12 ps. NPT equilibration at 10 K followed for 12 ps, again with restraints on solute heavy atoms. Next, NPT equilibration at 300 K was run for 12 ps with restraints on solute heavy atoms, and then again at 300 K with no restraints for 24 ps. The simulations for each receptor-ligand system were run for 100 ns with an NPT ensemble class set for a temperature of 300 K and a pressure of 1.01325 bar. The trajectories from each of these simulations were used to visualize the system over the thousand frames, and were processed with the Desmond Simulation Interactions Diagram.

MMGBSA studies

The free energy calculations of each receptor-ligand complex were determined using the molecular mechanics generalized Born surface area (MMGBSA) method by utilizing the prime module of Schrodinger Suite [56]. This module uses the trajectories of each receptor-ligand complex over the 100 ns simulation to calculate the free energy of the complexes as well as the ligand strain energy in a solution created by VSGB 2.0 suite [57]. MMGBSA uses solvation models and molecular mechanics calculations in order to determine the approximate free energies of the system [58]. The free energy of binding calculation is summarized by the equation $\Delta G_{bind}solv = \Delta G_{bind}vacuum + \Delta G_{solv}$ complex $- (\Delta G_{solv}$, ligand $+ \Delta G_{solv}$,receptor), with ΔG_{solv} being the sum of solvation energies of the free

ligand and receptor subtracted from the solvation energy of the receptor-ligand complex.

Pharmacokinetic analysis (ADMETlab 2.0)

The web server ADMETlab 2.0 was used to predict the pharmacokinetic properties of each of the compounds involving absorption, distribution, metabolism, excretion, and toxicity [59]. Membrane permeability, LogP, Pgp inhibitor/substrate, intestinal absorption, blood brain barrier permeation, HERG blocker were predicted to evaluate the conjugates and peptides.

Laboratory methods

Materials

The Melanocyte Inhibiting Factor-1 (MiF-1) and Neuropeptide FF (NPFF) were custom ordered from GenScript (Piscataway, NJ, USA). N-hydroxysuccinimide (NHS), 1-ethyl-3-(3-dimethylaminopropyl) carbodiimide (EDAC), Dimethyl sulfoxide-d6 (DMSO-d6) with 0.03% TMS, Gelatin from cold water fish skin, and Dimethylformamide (DMF) were purchased from Sigma Aldrich (St. Louis, MO, USA). Human Plasma Fibronectin was purchased from GIBCO, Life Technologies Corporation (Grand Island, NY, USA). 1X Dulbecco's Phosphate Buffered Saline (PBS) was purchased from ATCC (Manassas, VA, USA). NOP/ORL1 opioid receptor membrane preparation was purchased from Fisher Scientific. Gold-coated Surface Plasmon Resonance chips were purchased from Platypus Technologies (Fitchburg, WI, USA). Gallic acid anhydrous was purchased from Chem-Impex International INC. (Wood Dale, IL, USA). Betanin was purchased from Sigma Aldrich USA. Sinapic acid was purchased from ChemCruz, Santa Cruz Biotechnology, Inc. (Dallas, TX, USA). Pomolic acid was bought from Selleck Chemicals (Radnor, PA, USA).

Preparation of conjugates

Each mono-conjugate of gallic acid, pomolic acid, and sinapic acid was synthesized by activating the carboxylic groups with *N*-Hydroxysuccinimide (NHS) (5 mM) and 1-Ethyl-3-(3-dimethylaminopropyl) carbodiimide (EDAC) (5 mM) for 1.5 h in dimethylformamide (DMF) according to previously established coupling methods [60]. Then the corresponding peptide was added at 1:1 ratio and allowed to react for 48 h at 4 °C. For the betanin conjugates, the tri-peptide conjugates were prepared for which each peptide was added at a 3:1 ratio in order to conjugate to all three carboxyl groups of betanin. The N-terminus of the peptides were conjugated with the carboxyl groups of gallic acid, sinapic acid, pomolic acid or betanin. Then the solvent was evaporated using a R-205 rotary evaporator. The product obtained was recrystallized from acetone and speed vacuumed until dry using a ThermoFisher Scientific Savant ISS110 SpeedVac Concentrator. We synthesized eight conjugates: betanin-tri-MiF-1, betanin-tri-NPFF, gallate-MiF-1, gallate-NPFF, pomolate-MiF-1, pomolate-NPFF, sinapate-MiF-1, and sinapate-NPFF. The formation of the products was confirmed by FTIR (data not shown) and ^{1}H NMR spectra taken using a Bruker 400 MHz NMR in DMSO-d6 solvent that contained 0.3% TMS. The ^{1}H NMR peaks obtained for each conjugate are given below.

a) Sinapate-MiF-1: δ 0.7 (6H, t); δ 1.3 (1H, m); δ 1.7 (2H, q); δ 1.9 (2H, m); δ 2.2 (2H, s); δ 2.5 (2H, t); δ 3.8 (6H, s); δ 3.4 (2H, q); δ 3.6 (2H, m); δ 3.9 (2H, s); δ 4.2 (1H, t); δ 4.5 (1H, t); δ 6.5 (2H, s); δ 7.1 (1H, d); δ 7.3 (1H, d); δ 7.5 (2H, s); δ 8.2 (1H, s); δ 8.8 (1H, s).
b) Gallate-MiF-1: δ 0.8 (6H, t); δ 1.5 (1H, m); δ 1.6 (2H, t); δ 1.8 (2H, m); δ 2.2 (2H, q); δ 3.3 (2H, t); δ 4.0 (2H, s); δ 4.2 (1H, t); δ 4.5 (1H, t); δ 6.4 (2H, d); δ 7.1 (2H, s); δ 8.3 (1H, s); δ 8.8 (1H, s); δ 9.2 (1H, s); δ 9.5 (2H, s).
c) Pomolate-MiF-1: δ 0.7 (6H, d); δ 0.9 (6H, d); δ 1.0 (6H, s); δ 1.1 (3H, d); δ 1.2 (7H, t); δ 1.3 (2H, t); δ 1.4 (1H, t); δ 1.5 (5H, m); δ 1.6 (4H, m); δ 1.7 (2H, d); δ 1.8 (1H, d); δ 1.9 (2H, t); δ 2.0 (2H, m); δ 2.1 (3H, s); δ 2.2 (4H, s); δ 2.3 (4H, t); δ 3.3 (2H, t); δ 4.0 (2H, s); δ 4.2 (1H, t); δ 4.4 (1H, t); δ 4.5 (1H, s); δ 5.9 (1H, s); δ 7.2 (2H, s); δ 8.3 (1H, s); δ 8.9 (1H, s).
d) Betanin-tri-MiF-1: δ 0.9 (18H, d); δ 1.3 (3H, m); δ 1.5 (1H, s); δ 1.8 (6H, d); δ 2.0 (6H, t); δ 2.3 (2H, d); δ 2.4 (6H, t); δ 2.8 (1H, s); δ 3.4 (6H, t); δ 3.5 (2H, d); δ 3.6 (2H, t); δ 3.9 (6H, s); δ 4.1 (1H, s); δ 4.5 (6H, m); δ 4.8 (3H, s); δ 5.1 (1H, s); δ 6.1 (1H, s); δ 6.8 (2H, s); δ 7.2 (6H, s); δ 9.1 (3H, s); δ 9.2 (1H, s).
e) Sinapate-NPFF: δ 0.8 (6H, d); δ 1.5 (3H, m); δ 1.8 (4H, t); δ 2.1 (10H, t); δ 2.4 (2H, t); δ 2.6 (2H, s); δ 3.1 (6H, d); δ 3.2 (2H, t); δ 3.5 (2H, t); δ 3.8 (6H, s); δ 4.4 (5H, t); δ 5.1 (3H, t); δ 6.6 (2H, s); δ 6.3 (1H, d); δ 6.5 (2H, s) δ 7.0 (4H, s); δ 7.1 (3H, d); δ 7.2; (14H, s); δ 7.4 (2H, d); δ 7.8 (1H, s); δ 8.4 (7H, s); δ 8.7 (1H, s).
f) Gallate-NPFF: δ 0.9 (6H, d); δ 1.5 (3H, m); δ 1.7 (4H, m); δ 1.9 (8H, m); δ 2.2 (2H, m); δ 2.9 (1H, s); δ 3.1 (2H, t); δ 3.4 (4H, d); δ 3.5 (2H, t); δ 4.4 (5H, t); δ 4.9 (2H, t); δ 6.4 (1H, s); δ 6.8 (2H, s); δ 7.1 (12H, s); δ 7.1 (2H, s); δ 7.2 (3H, d); δ 7.4 (4H, s); δ 7.8 (1H, s); δ 8.7 (1H, s); δ 8.3 (6H, s); δ 8.8 (1H, s); δ 8.9 (1H, s). δ 9.2 (2H, s).
g) Pomolate-NPFF: δ 0.8 (15H, s); 0.9 (8H, d); δ 1.0 (1H, t); δ 1.2 (3H, s); δ 1.3 (1H, s); δ 1.5 (11 H, m); δ 1.6 (6H, t); δ 1.7 (6H, m); δ 1.8 (2H, d); δ 1.9 (4H, t); δ 2.2 (10H, t); δ 2.4 (2H, m); δ 2.7 (1H, s); δ 3.3 (3H, t); δ 3.5 (6H, d); δ 3.6 (2H, t); δ 4.5 (5H, t); δ 4.8 (3H, t); δ 5.0 (1H, s); δ 5.2 (1H, s); δ 6.7 (2H, s); δ 7.0 (4H, s); δ

7.1 (12H, s); δ 7.2 (3H,); δ 7.4 (2H, s); δ 7.9 (1H, s); δ 8.5 (6H, s).

h) Betanin-tri-NPFF: δ 0.8 (18H, d); δ 1.2 (2H, d); δ 1.3 (3H, m); δ 1.4 (3H, m); δ 1.4 (2H, m); δ 1.5 (4H, m); δ 1.6 (4H, m); δ 1.7 (2H, t); δ 1.8 (5H, m); δ 1.9 (10H, m); δ 2.0 (8H, m); 2.1 (1H, t); δ 2.2 (2H, t); δ 2.3 (6H, q); δ 2.4 (4H, t); δ 2.5 (4H, t); δ 2.7 (1H, d); δ 2.9 (2H, d); δ 3.0 (17H, d); δ 3.1 (6H, t); δ 3.2 (2H, d); δ 3.3 (2H, t); δ 3.4 (2H, d); δ 3.5 (2H, t); δ 3.6 (2H, t); δ 3.7 (2H, t); δ 3.8 (1H, t); δ 3.9 (3H, m); δ 4.0 (3H, t); δ 4.1 (1H, t); δ 4.2 (1H, t); δ 4.3 (11H, t); δ 4.4 (2H, t); δ 4.5 (2H, t); δ 4.6 (4H, t); δ 4.9 (1H, t); δ 5.1 (1H, d); δ 5.3 (4H, s); δ 6.2 (2H, d); δ 6.5 (6H, s); δ 7.0 (13H, s); δ 7.1 (2H, d); δ 7.1 (4H, d); δ 7.2 (12H, m); δ 7.3 (3H, d); δ 7.4 (12H, d); δ 7.5 (9H, d); δ 7.6 (6H, d); δ 7.8 (3H, s); δ 7.9 (1H, s); δ 8.2 (21H, s); δ 8.8 (1H, d).

Characterization

Surface plasmon resonance (SPR)

Gold-coated SPR chips (Platypus Technologies) were soaked in ethanol in a petri dish and placed under UV light for ten minutes. The chips were then coated with mixture of fibronectin (4 µg/mL) and gelatin (200 µg/mL) and stored for 24 h at 4 °C. After 24 h, the gold chips were coated with NOP/ORL1 opioid receptor membrane (25 µg/mL) (Eurofins Discoverex ChemiScreen NOP/ORL1 opioid receptor membrane preparation, purchased from Fisher Scientific). The chips were incubated in a 6 well plate for 2 h at 4 °C. Then the coated chips were stabilized in 3 mL of a HEPES-buffer solution consisting of 20 mM HEPES, 120 mM NaCl, 5.3 mM KCl, 1.8 mM $CaCl_2$, 0.8 mM $MgSO_4$, and 11.1 mM dextrose as described in previously established methods [61]. The coated chip was then spotted with one drop of Cargill's 7.21 index fluid, pressed to the SPR prism, and inserted into the SPR instrument (GWC Horizon SPR Imager II Instrument). The optimal angle for the run was adjusted and a 1X PBS solution was run through the instrument until SPR intensity values were stable and less than or near equal to zero.

Then, each of the samples were injected into the SPR at different concentrations (100 nM, 1 µM, 25 µM, 50 µM and 100 µM) to determine the optimal binding affinity. On average each run was conducted for 1000–1200 s and then switched with the buffer. Each run was repeated in triplicate. Chips were switched when each new conjugate or peptide was introduced. The flow rate was kept constant at 30 µL/min. The KD values were calculated using GraphPad Prism 9.5.0 software by running nonlinear regression analysis. Values reported are averages of three separate runs.

Statistical Analysis: We used Student's T-tests to carry out statistical analysis. In general P-values < 0.01 were considered statistically significant.

Results and discussion

Sigma profiles

Sigma profiles display the probability distribution of specific charge densities of a molecular surface area using quantum mechanical calculations and can provide vital information about hydrogen bond donor/acceptor capabilities as well as predict solubilities of potential pharmacological compounds in different solvent systems using COSMO-RS based methods [62, 63]. The sigma profiles of each of the conjugates and peptides were obtained from COSMO-RS (Fig. 2). The sigma profiles and the sigma surfaces of the NPFF conjugates and neat NPFF peptide are depicted in Fig. 2a. In the region below − 0.0082 e/Å^2, the peaks represent the hydrogen bond

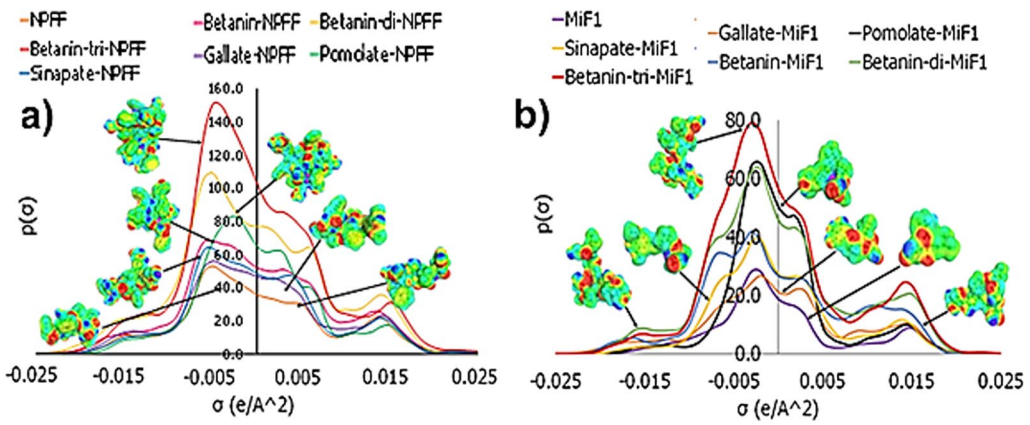

Fig. 2 Comparison of Sigma Profiles and Sigma Surfaces of (**a**) NPFF and its conjugates and (**b**) MiF-1 and its conjugates. Red indicates H-bond acceptor; green indicates non-polar and blue indicates H-bond donor regions on the sigma surfaces

donor region. As seen in the figure, betanin-tri-NPFF exhibits the highest of hydrogen bond donating ability. This is attributed to the fact that betanin-tri-NPFF has multiple hydroxyl groups and also contains three NPFF peptide moieties connected to the carboxyl groups via amide bonds. In the hydrogen bond accepting region, relatively larger peaks for all molecules are observed compared to H-Bond donor region. The betanin-tri and di-NPFF conjugate molecules showed higher peaks compared to the others due to the presence of the additional amide groups from the peptide moieties conjugated to betanin. The largest peaks appear in the hydrophobic region between − 0.0082 e/Å^2 to + 0.0082 e/Å^2. Betanin-tri-NPFF displayed the strongest peak because of the presence of three NPFF peptide moieties. NPFF (FLFQPQRFa) itself is a hydrophobic peptide and incorporation of three of those renders the conjugates more hydrophobic. As expected, betanin-di-NPFF has the next highest hydrophobic peak. The pentacyclic triterpene conjugate, pomolate-NPFF, was found to be slightly more hydrophobic compared to betanin-mono-NPFF, though the two peaks are relatively close due to the presence of the hydrophobic terpene ring system. The corresponding sigma surfaces depict the areas of the charge densities on each of the molecules, with red being the H-bond acceptor region, blue representing hydrogen bond donor region and green displaying hydrophobic region.

Figure 2b shows a comparison of the sigma profiles and sigma surfaces of the MiF-1 conjugates and the neat MiF-1 peptide. Overall, compared to the NPFF conjugates, the MiF-1 conjugates showed lower ρ(s) values, though similar trends were observed. In the hydrophobic region the betanin-tri-MiF-1 conjugate showed the highest hydrophobicity and the neat peptide showed the lowest peak in the hydrophobic region. MiF-1 (Pro-Leu-Gly-NH_2) is a shorter peptide sequence and contains no aromatic ring systems (unlike NPFF), which attributes to the lower hydrophobicity. In the hydrogen bond accepting region, relatively higher peaks were seen for betanin-di-MiF-1 and betanin-tri-MiF-1 due to the presence of the additional amide groups from the di- and tripeptide conjugates. The hydrogen bond donating region also showed slightly higher peaks for the betanin-di-MiF-1 and betanin-tri-MiF-1 conjugates. All of the other conjugates and the peptide alone showed relatively similar intensity in this region. Overall, in the case of both MiF-1 and NPFF conjugates, incorporation of the phytochemicals resulted in increased hydrophobicity as well as hydrogen bond accepting capability. These properties may play a key role when binding to the receptor. We then compared the sigma profile and surface with the endogenous peptide N/FQ sequence (FGGFTGARKSARKLANQ). As shown in Additional file 1: Figure S1, results indicate that the ρ(s) value for the N/FQ sequence was closer in value to that of the betanin-Tri-MiF1 and betanin-tri-NPFF conjugate. It was also found to have a similar peak in the hydrogen bond acceptor region, though the peak in the hydrogen bond donor region was relatively higher and broader for the N/FQ sequence due to the presence of Arg and Lys moieties in the peptide.

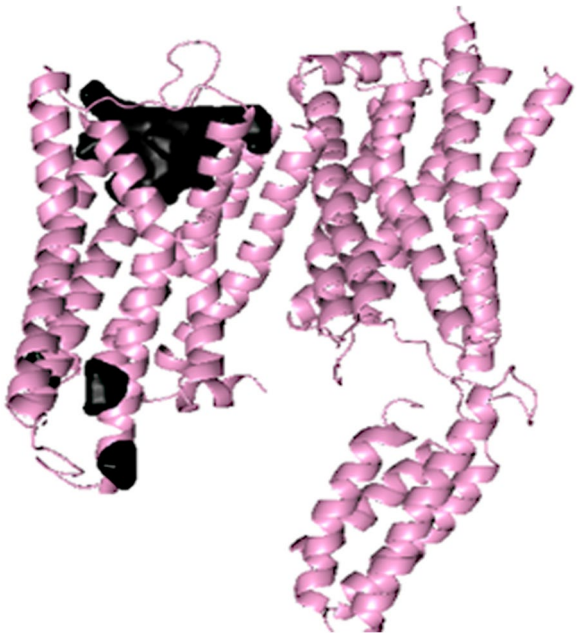

Fig. 3 Binding pocket analysis of NOPR using POCASA. Pockets are shown in black

Table 1 Binding pocket analysis of NOPR using POCASA

Rank number	Pocket number	Volume (Å)	VD
1	122	700	2665
2	281	42	100
3	32	34	73
4	287	29	70
5	339	20	49

Cleft determination

The POCASA web server was used to examine the binding pocket of both NOP receptor. Results obtained are shown in Fig. 3 and Table 1. The volume depth (VD) of each pocket compares depth, position, and volume in order to predict the most optimal pocket. Table 1 shows that NOPR displayed a total of five pockets, and the optimal binding pocket was predicted to have a volume of 700 Å and VD value of 2665.

Molecular docking studies

To determine the binding interactions of the conjugates and the peptides with the receptor, molecular docking studies were conducted. Results of the binding affinities obtained are shown in Table 2**.** In the case of NPFF and its conjugates, the pomolate-NPFF conjugate showed the highest binding affinity (− 9.0 kcal/mol). Betanin-tri-MiF-1, sinapate-NPFF, and pomolate-MiF-1 also showed good binding affinities at − 8.6 kcal/mol, − 8.5 kcal/mol, and − 8.3 kcal/mol, respectively. The binding affinity of NPFF alone was relatively high at − 8.0 kcal/mol compared to the NF/Q endogenous peptide sequence which showed a binding affinity of − 6.0 kcal/mol which is closer to that seen of MiF-1 neat peptide at − 6.8 kcal/mol. The specific interactions occurring within the binding pockets of the docked receptor-ligand complexes were visualized using PLIP and are shown in Fig. 4 and Additional file 1: Table S1.

The neat NPFF peptide formed eight hydrogen bonds with residues including Lys51, Asp130, Cys200, Gln286, Gln291, and Arg302; seven hydrophobic interactions with Val126, Ile127, Pro292, Val298, Ala299 and Leu301; and one salt bridge with Asp110. In previous studies it has been shown that the NOP antagonist C-24 also showed interactions with Asp130 and Arg302 residues of the transmembrane helices TM3 and TM7 which are within the orthosteric binding pocket of the NOPR [50]. In addition, interactions are also seen with Gln286 and Gln291 from TM6 and Cys200 from ECL2 region. Furthermore, when comparing with the binding interactions with the endogenous ligand N/FQ from previous work, [64] it was shown that Asp130, Gln286, Cys200, Arg302 are involved in binding. Thus, NPFF appears to bind within the expected binding pocket of the NOP receptor, in addition to making additional new hydrophobic interactions with residues such as Val298, Ala299, Leu301 within the TM7 helix region which facilitate binding.

Table 2 Binding affinities for each peptide and conjugate with NOPR (kcal/mol) obtained using AutoDock Vina

Peptide/Conjugate	Binding affinity (Kcal/mol)
NPFF	− 8.0
Gallate-NPFF	− 7.8
Pomolate-NPFF	− 9.0
Sinapate-NPFF	− 8.5
Betanin-mono-NPFF	− 7.5
Betanin-di-NPFF	− 7.1
Betanin-tri-NPFF	− 7.8
MiF-1	− 6.8
Gallate-MiF-1	− 6.9
Pomolate-MiF-1	− 8.3
Sinapate-MiF-1	− 7.4
Betanin-MiF-1	− 7.6
Betanin-di-MiF-1	− 7.6
Betanin-tri-MiF-1	− 8.6
FGGFTGARKSARKLANQ	− 6.0

The conjugates showed an increase in the number of interactions, specifically hydrophobic interactions, in all cases and in some cases, a reduction in hydrogen bond interactions compared to neat NPFF. The gallate-NPFF conjugate displayed fourteen hydrophobic interactions including those with Ile317 and Phe321 in the core TM7 region, as well as with residues such as Val52, Val59 and Val55 in the TM1 region and Phe115 in the TM2 region. The number of hydrogen bonds was found to be six primarily with Ala60, Gly64, Gly68 and Pro105. Specifically, Gly64 and Gly68 belong to the hinge region of NOPR and have been known to play an important role in ligand binding. As expected, the pomolate-NPFF conjugate showed significantly more hydrophobic interactions (twenty-one), though the number of hydrogen bonds was lower (five) compared to the neat peptide. The hydrophobic interactions were seen primarily with residues Phe303, Leu307, Val310, Ala320, Phe321, and Phe330 located in the TM7 helix region and with residues Thr109, Leu112, Leu113 occurring in the TM2 region. Additional interactions were seen with Val55, Leu57, Leu59, Val63, Leu67, Leu71 in the TM1 region. The five hydrogen bonds seen with residues Thr53, Gly56, Leu57, and Leu59 primarily occurred in the TM1 region. Interestingly, the interactions with Asp130, Cys200 and Arg302 were no longer seen. Sinapate-NPFF showed a similar pattern in that once again hydrophobic interactions (twenty-one) played a significant role in binding with TM1, TM2 and TM7 helices and only two hydrogen bonds were found with residues Thr53 from TM1 and Gly64 from the hinge region. Betanin-tri-NPFF showed 39 hydrophobic interactions with residues in the NOPR binding pocket including those with residues Thr109, Phe115, Ile127, Glu295 and Ile317, which is expected given the large size of the ligand, with three NPFF peptide moieties conjugated to betanin. Furthermore, hydrogen bond interactions with Arg302 were also seen. The number of hydrophobic interactions was found to decrease as the number of NPFF moieties conjugated was reduced (twenty-seven for betanin-di-NPFF and sixteen for the betanin-mono-NPFF conjugate). The number of hydrogen bonds were found to be six, six, and eleven respectively for the mono, di and tri-NPFF conjugates of betanin. Furthermore, stacking interactions were observed for all the three betanin-NPFF conjugates with Phe330 residue of the NOP receptor. Thus overall, for

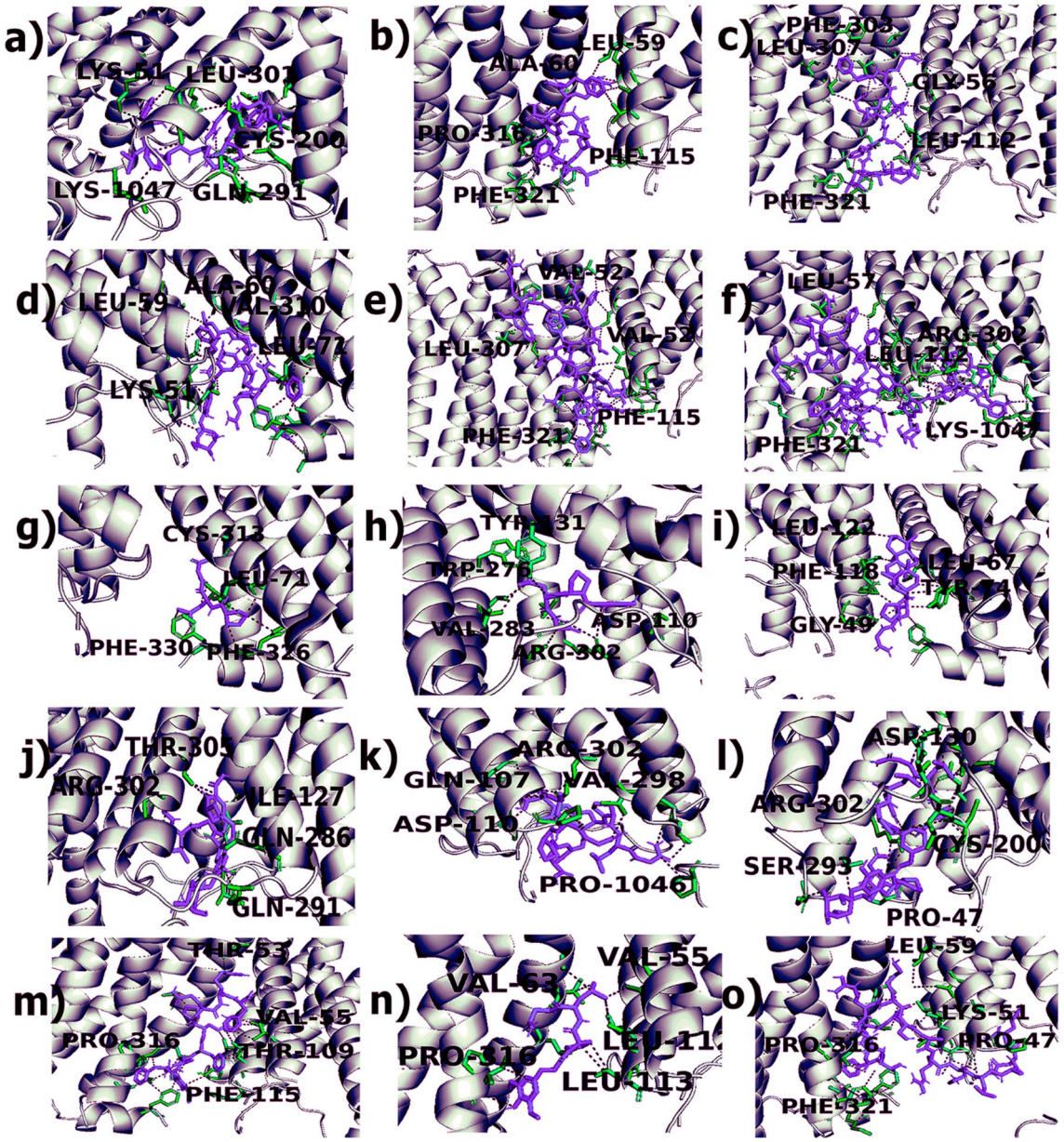

Fig. 4 Binding pocket interactions from PLIP analysis for NPFF and MiF-1 conjugates as well as the neat peptides. The ligand (conjugate or peptide) is shown in purple. Interacting residues of NOPR are shown in green. (**a**) NPFF; (**b**) Gallate-NPFF; (**c**) Pomolate-NPFF; (**d**) Betanin-NPFF; (**e**) Betanin-di-NPFF; (**f**) Betanin-tri-NPFF; (**g**) MiF-1; (**h**) Gallate-MiF-1; (**i**) Pomolate-MiF1; (**j**) Betanin-MiF-1; (**k**) Betanin-di-MiF-1; (**l**) Betanin-tri-MiF-1 (**m**) Sinapate-NPFF; (**n**) Sinapate-MiF1; (**o**) FGGFTGARKSARKLANQ

the NPFF conjugates, the ligands appear to be interacting within the central core of the receptor and are mainly pointing toward helices TM1, TM2, and TM7, within a hydrophobic environment. Similar results were seen with recently developed NOP antagonists such as BTRX-246040 [65].

The docking results of MiF-1 and its conjugates with NOPR indicated that neat MiF-1 peptide alone had a moderate binding affinity of − 6.8 kcal/mol. The lower binding affinity compared to NPFF could be attributed to the lack of aromatic amino acid groups as well as charged residues which mimic the endogenous peptide more closely. Upon conjugation, the MiF-1 conjugates showed relatively higher binding affinities. The highest increases were seen in the case of betanin-tri-MiF-1 with an affinity of − 8.6 kcal/mol and pomolate-MiF-1, with an affinity of − 8.3 kcal/mol. As seen, the PLIP results for MiF-1 displayed two hydrogen bonds with residues Cys313 and

Phe326 in the TM7 region, as well as seven hydrophobic interactions with residues Leu71, Val72, Ile317, Phe326, and Phe330 encompassing TM1 and TM7 helices. In contrast, Betanin-tri-MiF-1 displayed ten hydrogen bonds with Pro47, Gln107, Asp130, Cys200, Ser293, Arg 302, and Tyr309, and nine hydrophobic interactions with residues including Gln107, Asp110, Val126, Ile127, Asp130, Leu201, Val202, and Val298 primarily from the TM2, TM3 and TM7 region. Similar key interactions have been reported for the well-known NOP receptor antagonist Cebranopadol that showed contacts with Asp130, Ile127 and Gln107 [66]. Similar to NPFF conjugates, the number of hydrophobic interactions was lesser for the mono and di-MiF-1 betanin conjugates (two and seven respectively) compared to the tri-MiF-1 betanin conjugate. Additionally, the number of hydrogen bonds were found to be seven and eight respectively for the mono and di-betanin-MiF-1 conjugates. Once again crucial interactions with Arg302 and Gln107 were seen in all cases. The pomolate-MiF-1 also displayed hydrophobic interactions with nine residues including residues such as Leu67, Tyr74, Phe115, Pro117, Phe118, and Leu122 which are primarily from the TM1, TM2 and TM3 region. Interestingly no interactions were seen with residues in the TM7 region and no hydrogen bonds were seen indicating that the pomolate-MiF-1 binds in a slightly different region of the receptor. The gallate-MiF-1 and the sinapate-MiF-1 conjugates displayed six and two hydrogen bonds respectively. The number of hydrogen bonds for the gallate conjugate is higher due to the presence of three free hydroxyl groups as opposed to sinapate where two of the hydroxyl groups are methoxylated. Overall the sinapate moiety is also more hydrophobic compared to gallate due to the presence of the prop-2-enoate moiety. Thus, the sinapate-MiF-1 conjugate showed higher number of hydrophobic interactions (nine) compared to gallate-MiF-1 which only showed four hydrophobic interactions. Notably, gallate-MiF-1 and betanin-mono-MiF-1 both interact with NOPR through a key hydrogen bond contact (Thr305) which is at the extracellular end of the binding pocket, making those ligands more selective toward NOPR compared to other opioid receptors which have an Ile residue at the same position as seen in the case of NOPR agonist Ro64-6198 [67]. Overall, the interactions seen were within the binding pocket of the NOP receptor with residues in the TM2, TM3, TM7 and TM1 region.

Generally, the MiF-1 conjugates seemed to make key interactions within the binding pocket, though in most cases the number of interactions were lower compared to the NPFF conjugates. However, NPFF conjugates showed a number of prominent hydrophobic and hydrogen bond interactions with the different TM domains. The endogenous peptide N/FQ comparatively showed fifteen hydrophobic interactions with residues such as Ile317, Ala320, Phe321 and eight hydrogen bonds as well as stacking interactions with Phe321.

Molecular dynamics simulations

To further investigate the binding interactions and for detailed perspective of the receptor-ligand complexes, we carried out molecular dynamics (MD) simulations over 100 ns (ns). The average Root Mean Square Deviations (RMSDs) obtained are shown in Table 3. In general, higher RMSD values were seen for the NPFF conjugates compared to the MiF-1 conjugates with the exception of betanin mono-MiF-1 and sinapate-MiF-1 conjugates which showed the highest RMSD value amongst all of the MiF-1 conjugates.

NPFF conjugates For the NPFF peptide and its conjugates, in most cases, (with the exception of pomolate-NPFF) the average value was lower for the ligand-receptor complexes compared to Cα, which implies that a more stable conformation was attained upon binding to each of the ligands. This is particularly evident for betanin mono-NPFF, di-NPFF and tri-NPFF conjugates where the RMSD value was found to be lowest for the betanin-tri-NPFF conjugate complex with NOPR. Interestingly, the neat NPFF did not show a significant difference between the Cα and ligand-receptor RMSD values (a difference of only 0.4 nm for the ligand receptor complex), while the pomolate-NPFF showed a difference of 0.1 nm. Similar

Table 3 Comparison of average RMSD values obtained for Designed Peptides and Conjugates with NOPR over 100 ns simulation

Peptide/Conjugate	Cα (nm)	Ligand-receptor complex (nm)
NPFF	1.519	1.141
Gallate-NPFF	1.651	0.903
Pomolate-NPFF	1.504	1.658
Sinapate-NPFF	1.700	1.137
Betanin-NPFF	2.317	1.453
Betanin-di-NPFF	1.183	0.370
Betanin-tri-NPFF	1.149	0.241
MiF1	1.049	1.287
Gallate-MiF-1	0.93	0.581
Pomolate-MiF-1	0.749	1.289
Sinapate-MiF-1	0.993	4.169
Betanin-MiF-1	2.97	2.620
Betanin-di-MiF-1	1.276	0.835
Betanin-tri-MiF-1	1.636	1.579
FGGFTGARKSARKLANQ	1.358	2.052

results were seen in previous studies where it was also demonstrated that the formation of complex of a NOP peptide with NOP receptor resulted in lower RMSD values compared to Cα of NOPR [68]. To further elucidate the interactions, we compared the trajectories (Fig. 5). As can be seen in the figure, for the neat peptide NPFF, interactions are primarily seen with residues from TM1, TM7 and TM2 region. Although the conformation of the ligand appears to change over the 100 ns simulation, a compact structure of the ligand is seen at the end of the simulation. Furthermore, the peptide NPFF remains attached to the receptor throughout the simulation. Additionally, NPFF peptide inflicts a conformational change in NOPR after 50 ns and TM domains appear to move closer to each other in order to accommodate the ligand within the binding pocket resulting in a conformation change. Interactions with Asp110, Asp130, Cys200, Gln286, Gln291, and Arg302 throughout the 100 ns simulation are seen. Gallate-NPFF also resulted in a conformation change of the NOPR after 50 ns, but remains stable after 50 ns with barely any movement of the ligand within the receptor. Pomolate-NPFF demonstrated limited movement, where the ligand appears to fold up within the TM helices after 50 ns and remains stable in that position. Pomolate-NPFF also shares the binding pocket with Gallate-NPFF with major interacting residues being Ala60, Cys313, and Ile317. Both of these conjugates attain higher contacts by 100 ns. Sinapate-NPFF shows drastic changes in the conformation for the first 50 ns, indicating that the complex formed is not stable initially, however it appears to attain a stable conformation after 50 ns. While betanin-di-NPFF causes NOPR to become slightly distorted from its original conformation initially, after 50 ns, minimal conformational changes occur. The other betanin-peptide conjugates remained stable throughout the simulation. This is likely because of the size of the conjugates which renders them less flexible within the binding pocket and they remain attached. Major interacting residues across all three betanin-NPFF conjugates included Leu112 and Cys313.

We then compared the radii of gyration and RMSF (Root Mean Square Fluctuations) for each of the NPFF conjugates when complexed with NOPR (Fig. 6). The betanin-tri and di-NPFF conjugates demonstrated the highest radii of gyration indicating comparatively less compactness (Fig. 6a). This is expected given the relatively larger sizes of those conjugates which are more spread out within the TM helices of the receptor. The Rgyr of betanin-tri-NPFF remained at around 1.2 nm throughout the simulation while that of betanin-di-NPFF was initially at 1.0 nm, and rose slightly to 1.1 nm at 60 ns. This indicates that the ligand became more extended over the course of the trajectory, and remained in this position until the end of the simulation. Considerable overlap occurred between pomolate-NPFF, sinapate-NPFF, and betanin-mono-NPFF. While betanin-mono-NPFF remained stable in this configuration with a nearly linear trend at 0.8 nm, sinapate-NPFF and pomolate-NPFF showed fluctuations initially with the Rgyr reducing from 0.8 to 0.6 nm by the end of the simulation indicating an increase in compactness at the later part of the simulation. The lowest Rgyr values were seen for gallate-NPFF and neat NPFF, due to their relatively smaller structures, which resulted in more compactness.

Comparison of the RMSF values for the receptor backbone throughout each simulation revealed that binding with both betanin-di-NPFF and betanin-tri-NPFF resulted in higher fluctuations (Fig. 6b). Specifically, betanin-tri-NPFF also showed smaller peaks around residues Met82, Ser164, Glu194, Gly244, Ser294, and Cys329 of the A chain, and His79, His154, Arg209, and Lys254 of the B chain. Betanin-di-NPFF also resulted in major fluctuations around residues His79, Leu113, Pro155, Glu194, and Thr296 of the A chain; Pro47, His79, Cys153, and Tyr210 of the B chain. The gallate-NPFF, pomolate-NPFF, and sinapate-NPFF resulted in increases of about 1.0 nm for the extracellular loop region, TM1 and TM2 residues, once again cementing this region as the area of greatest fluctuation. Fluctuations were also seen around Lys83, Ser164, Glu194, Tyr210, and Ser294 of the A chain, and Pro47, Lys81, Ile111, Pro155, Tyr210, and Lys254 of the B chain, though these residues exhibited limited fluctuation.

We also examined the protein–ligand contacts for each of the NPFF conjugates with NOPR (Additional file 1: Fig S2). For the neat NPFF peptide, we observed an average of about 20 contacts across the simulation. The major interactions were predominantly hydrogen bonds and water bridges, specifically a hydrogen bond and water bridge with Asp130 of magnitude 3.0 interaction fraction, a water bridge and hydrogen bond with Cys200 with an interaction fraction of 2.75, and a hydrogen bond with Asp110 with 2.0 interaction fraction indicating that those residues played a major role in binding with NPFF. Most conjugates showed slightly lower number of contacts over the 100 ns simulation with gallate-NPFF displaying an average of 14 contacts, interacting predominantly through hydrogen bonds and water bridges; however, higher number of hydrophobic contacts with residues such as Ile317, Val310 and Phe330 were seen. Sinapate-NPFF showed a similar pattern as that of gallate-NPFF and averaged about 13 contacts. Highest interaction fractions were seen for Arg331, Phe330 and Phe115. Pomolate-NPFF showed on average 10 contacts over the course of the simulation, with its largest interaction fraction being 0.8 which accounted for a water bridge with

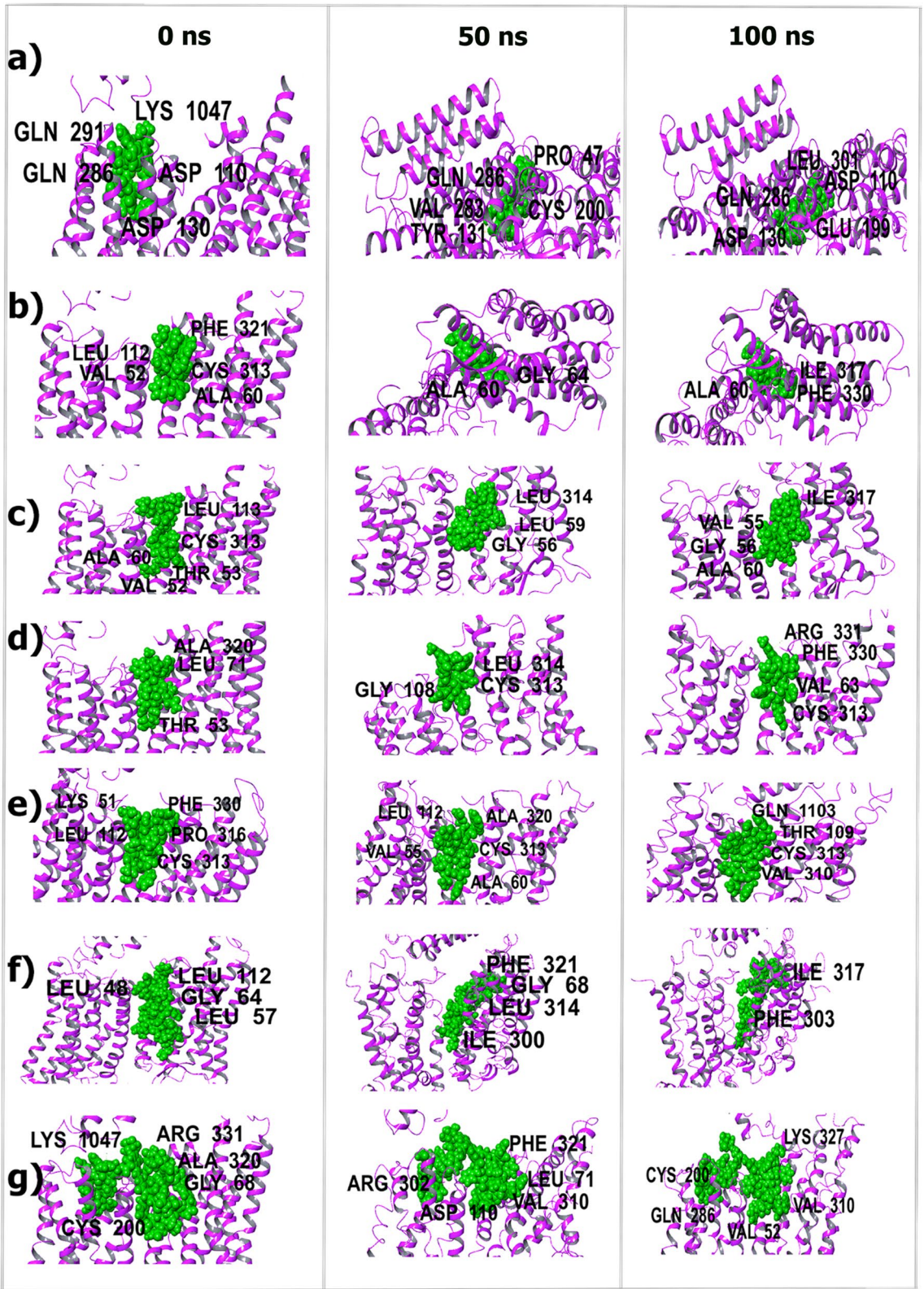

Fig. 5 Trajectory images for Molecular Dynamics Simulations with NOP Receptor with NPFF and its conjugates at 0, 50, and 100 ns. (**a**) NPFF; (**b**) Gallate-NPFF; (**c**) Pomolate-NPFF; (**d**) Sinapate-NPFF; (**e**) Betanin-mono-NPFF; (**f**) Betanin-di-NPFF; (**g**) Betanin-tri-NPFF. Each ligand is represented in green and the receptor is indicated in purple

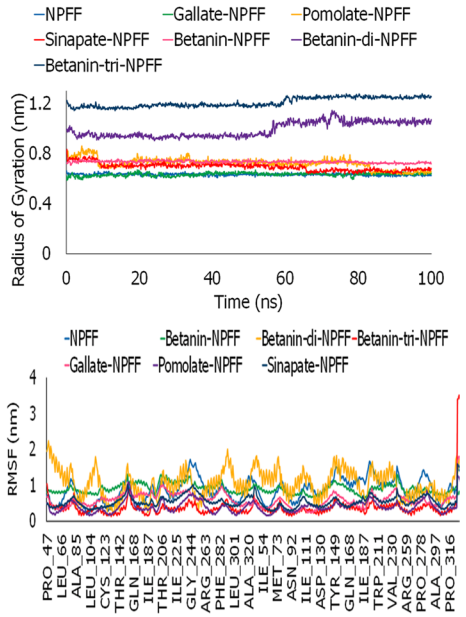

Fig. 6 Comparison of radius of gyration (top) RMSF (bottom) for NPFF and its conjugates when complexed with NOPR

Cys313 and a significant number of hydrophobic interactions with residues such as Ile317 and Leu314. Betanin-mono-NPFF showed an increase in contacts steadily as the simulation progressed. For both betanin-di-NPFF and betanin-tri-NPFF, we were unable to obtain protein–ligand contact data due to software limitation and size of the ligand-receptor complex. Instead, we determined the contributions of the types of interactions, which showed higher interactions with the betanin-tri-NPFF compared to betanin-di-NPFF, with hydrogen bond interactions playing a major role.

MiF-1 conjugates The average RMSD for Gallate-MiF-1 complex with NOPR was found to be the lowest while sinapate-MiF-1 complex displayed the highest RMSD value (least stable). It is likely that the propene-2-ene moiety of sinapate may add additional flexibility to the ligand resulting in higher movement of the ligand within the receptor. In addition, amongst the betanin complexes, all conjugates showed lower RMSD values for the ligand-receptor complexes compared to corresponding Cα indicating that the receptor is stabilized upon binding to those ligands. Furthermore, the RMSD values were highest for the betanin-mono-MiF-1 complex and lowest for the betanin-di-MiF-1 complex, while the tri-MiF-1 conjugate showed intermediate stability. To further decipher these results, we analyzed the trajectories. As seen in Fig. 7, the MiF-1 neat peptide and pomolate-MiF-1 bind within the hydrophobic core of TM helices making interactions with residues such as Ala320, Ile317 and Pro117. Pomolate-MiF-1 was found to attach to the binding pocket and then moved further down making contacts with the TM helices. Gallate-MiF-1 which formed the most stable complex of all of the MiF-1 conjugates remained bound to the binding pocket making key interactions with residues Asp110, Asp130, Gln286, Gln280, and Thr305. As expected, the sinapate-MiF-1 conjugate shows significant movement throughout the simulation, and is not nestled within the binding pocket. During the course of the simulation it goes further deep down into the hydrophobic region of the transmembrane helices making contacts with TM2 and TM3 hydrophobic residues such as Val161 and Leu177 toward the end of the simulation, thus moving away from the binding pocket. The betanin conjugates appear to bind in the region between ECL2, TM2 and TM3. The betanin-mono-MiF-1 conjugate shows key contacts with Asp130, Gln286, Val202 and Tyr309. The betanin-di-MiF-1 conjugate appeared to remain within the binding pocket, with minimal movement, making contacts with key residues Cys200, Gln107, Gln291 and Val298 by the end of the simulation. The betanin-tri-MiF-1 conjugate on the other hand makes key contacts with Asp130, Asp110, Phe215 and remains stable throughout the simulation.

The corresponding radius of gyration and RMSF results are shown in Fig. 8. The radius of gyration values overall were found to be lower for the MiF-1 conjugates compared to the NPFF conjugates, (Fig. 8a) though the trends were similar. Betanin-tri-MiF-1 conjugate showed the highest Rgyr, at 0.8 nm. Interestingly, however, both betanin-di-MiF-1 and betanin-mono-MiF-1 nearly overlap at 0.65 nm; given their size differences, this suggests that betanin-di-MiF-1 is maintaining a more constricted conformation throughout the simulation. Sinapate-MiF-1 demonstrated the most changes in Rgyr over the course of the simulations especially in the first 50 ns, after which it appears to stabilize at 0.52 nm. The pomolate-MiF-1 however remained consistently at 0.5 nm for the simulation. Both gallate-MiF-1 and the neat peptide MiF-1 remained stable around 0.4 nm for the entirety of the simulation, with the gallate-MiF-1 conjugate displaying a slightly higher Rgyr value than the neat MiF-1 peptide as expected, given that MiF-1 is the smallest ligand studied and therefore most compact structure.

The results of RMSF indicate that the highest fluctuations of the NOP receptor backbone were seen when bound to betanin-mono-MiF-1 at residues Leu113, Ile198, and Ser294 of the A chain; and Lys51, Gly114, Cys200, and Ala297 of the B chain. Betanin-tri-MiF-1 showed the next highest fluctuation at residues Glu324, Gln107, Asp209 and Ser294. The RMSF values for the neat peptide MiF-1, gallate-MiF-1, pomolate-MiF-1, sinapate-MiF-1, and betanin-di-MiF-1 remained relatively similar for all of the residues, with minimum fluctuations

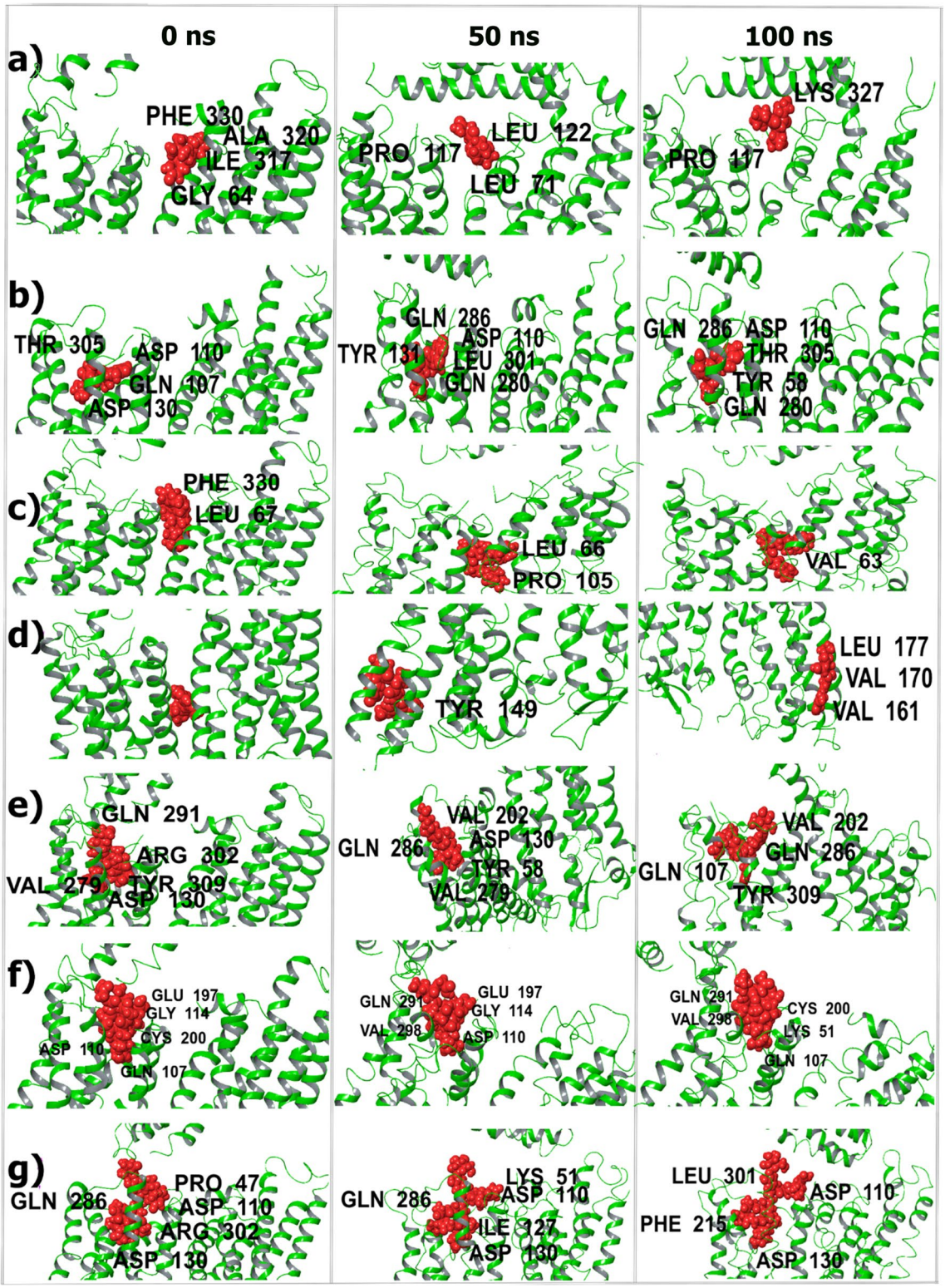

Fig. 7 Trajectory images of NOPR with MiF-1 and its conjugates at 0, 50, and 100 ns. (**a**) MiF-1; (**b**) Gallate-MiF-1; (**c**) Pomolate-MiF-1; (**d**) Sinapate-MiF-1; (**e**) Betanin-mono-MiF-1; (**f**) Betanin-di-MiF-1; (**g**) Betanin-tri-MiF-1. The receptor is shown in green, while the ligands are indicated in blue

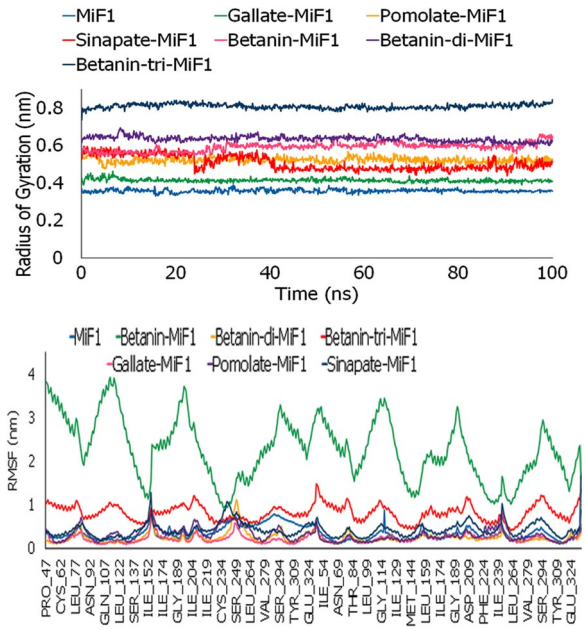

Fig. 8 Comparison of radius of gyration (top) RMSF (bottom) for MiF-1 and its conjugates when complexed with NOPR

between 0.5 and 0.6 nm with particular peaks around Ile152, Ser249, Ile54, Ser294 and Ile129. Overall relatively less fluctuation was observed for the MiF-1 conjugates compared to the NPFF conjugates.

Upon examining the protein–ligand contacts (Additional file 1: Fig S3), results indicate an average of five contacts for the neat MiF-1 peptide, however, over the course of the simulation, the number of contacts increased to seven indicating an increase in interactions. Primary interactions involved hydrogen bonds, water bridges, and hydrophobic interactions. However, its interaction fractions only reached a maximum of 0.7. The greatest number of contacts was seen for betanin-tri-MiF-1 with an average of 20 contacts and a maximum interaction fraction of about 2.25. Its major interactions included hydrogen bonds and water bridges with Asp130, Gln107, and Thr305. Betanin-di-MiF-1 had similar contacts, averaging about 19 contacts throughout the simulation and having major interactions with Asp110, Cys200, and Arg302. Gallate-MiF-1 showed an average of 14 contacts throughout the simulation. It also had a hydrophobic interaction and water bridges with Asp110 at an interaction fraction of 2.0. The pomolate-MiF-1 conjugate showed the lowest number of contacts at an average of 3, although for the first 10 ns the number of contacts was 8; however, over the course of simulation the number of contacts decreases to an average of 2–3 indicating that the ligand is no longer in the binding pocket. Sinapate-MiF-1 was slightly better than the pomolate-MiF-1 conjugate, however the average number of contacts was found to be five over the course of the simulation. Interactions with Tyr149, Val146 and Arg157 were seen. For both the NPFF and MiF-1 conjugates, the most optimal results were seen for betanin-di-NPFF, betanin-tri-NPFF, gallate-MiF-1, and betanin-di-MiF-1 while pomolate-NPFF showed intermediate results.

We also conducted MD simulations with the endogenous peptide (FGGFTGARKSARKLANQ)-NOPR complex in order to compare the binding interactions with those of the designed conjugates. The results are shown in Additional file 1: Fig S4. As expected, the ligand remains firmly attached to the receptor within the binding pocket making contacts with Leu113, Lys51, Glu295. There appears to be slight conformation changes occurring for the ligand, but overall, it remains attached to the binding pocket with minimal movement. We next examined the Rgyr and RMSF data for the FGGFTGARKSARKLANQ-NOP receptor complex. As seen, the Rgyr reduces from 0.90 to 0.81 within the first 20 ns after which it remains steady up to 90 ns and then further reduces to 0.80 ns by the end of the simulation indicating that the ligand becomes more compact over the course of the simulation. The RMSF results indicate that residues which show more fluctuation include Phe118, Asp209, Leu48, Glu197 and Ser293. These results indicate that the designed peptide conjugates such as Gallate-MiF-1, the betanin di and tri conjugates appear to bind within the same region. While the binding was not as stable for sinapate-MiF-1 it does initially also bind to the same region as well.

MMGBSA studies

The molecular mechanics generalized Born surface area (MM-GBSA) provides an accurate prediction about the binding free energy of protein–ligand binding over the entire simulation compared to other scoring functions such as molecular docking [69]. The results of the various ligands with NOPR are shown in are also shown in Table 4. The highest binding affinity among NPFF and its conjugates was found to be for betanin-di-NPFF (− 89.2 kcal/mol) and betanin-tri-NPFF (− 90.2 kcal/mol), while that of neat NPFF was found to be − 85.7 kcal/mol. Gallate-NPFF showed a lower binding energy of − 50.6 kcal/mol, while pomolate-NPFF displayed a ΔG bind of − 57.3 kcal/mol. Overall, van der Waals forces contributed significantly to binding energy.

MiF-1 and its conjugates showed higher ΔG binding energy for all of the conjugates compared to the neat MiF-1 peptide alone (− 29.5 kcal/mol). The low ΔG_{bind} for the neat MiF-1 peptide is expected given that it is a short three-amino acid peptide and did not form a

Table 4 MMGBSA analysis

Peptide/Conjugate	Average G binding energy (kcal/mol)	Average H-bond energy (kcal/mol)	Average lipophilic energy (kcal/mol)	Average vdW energy (kcal/mol)
NPFF	− 85.7	− 4.5	− 20.6	− 67.8
Gallate-NPFF	− 50.6	− 1.2	− 20.7	− 42.3
Pomolate-NPFF	− 57.3	− 0.2	− 23.2	− 57.6
Sinapate-NPFF	− 74.9	− 0.9	− 26.6	− 65.6
Betanin-NPFF	− 82.5	− 1.7	− 26.7	− 68.2
Betanin-di-NPFF	− 89.2	− 1.1	− 35.4	− 83.6
Betanin-Tri-NPFF	− 90.2	− 1.8	− 38.4	− 87.8
MiF-1	− 29.5	− 0.66	− 9.7	− 27.2
Gallate-MiF-1	− 68.0	− 2.98	− 16.3	− 45.8
Pomolate-MiF-1	− 31.2	− 0.1	− 14.5	− 29.1
Sinapate-MiF-1	− 30.9	− 0.46	− 10.9	− 26.3
Betanin-MiF-1	− 75.9	− 2.4	− 16.8	− 61.6
Betanin-di-MiF-1	− 74.9	− 3.2	− 16.2	− 63.9
Betanin-tri-MiF-1	− 85.4	− 3.3	− 20.0	− 86.0
FGGFTGARKSARKLANQ	− 54.8	− 2.86	− 18.5	− 59.1

stable complex as described earlier. Betanin-tri-MiF-1 was found to be the most optimal candidate among these conjugates, with a binding energy of − 86.0 kcal/mol, while the corresponding di- and mono-MiF1 conjugates of betanin also showed relatively high ΔG binding energies of − 74.9 kcal/mol and − 75.9 kcal/mol. The gallate conjugate also showed fairly high ΔG bind at − 68.0 kcal/mol. The pomolate-MiF-1 and sinapate-MiF-1 displayed significantly lower binding energies compared to the above conjugates which corroborates with the simulation trajectories seen. The highest binding energy contributions were found to be from hydrophobic and van der Waals energy. Overall, the most optimal binding energies for the NOP receptor were found to be with betanin-di-NPFF and betanin-tri-MiF-1 as shown in Table 4.

Pharmacokinetics predictions

We utilized the web server ADMETlab 2.0 to analyze the pharmacokinetic properties of the conjugates in

Table 5 Pharmacokinetic properties of NPFF and MiF-1 and conjugates

Peptide/ Conjugate	logP	Human intestinal absorption	BBB penetration	PgP inhibitor	PgP substrate	Pfizer rule	MDCK permeability	hERG blockers
NPFF	0.884	0.994	0.003	0.912	0.503	Accepted	9.25E-05	0.03
Betanin-NPFF	− 0.054	1	0.005	0	0.695	Accepted	4.47E-05	0.006
Betanin-di-NPFF	1.056	1	0	0	0.294	Accepted	1.66E-05	0
Betanin-tri-NPFF	2.574	1	0	0	0.149	Accepted	1.53E-05	0
Gallate-NPFF	0.806	1	0.001	0.192	0.852	Accepted	4.52E-05	0.016
Pomolate-NPFF	4.199	0.932	0.003	1	0.014	Accepted	1.34E-04	0.018
Sinapate-NPFF	1.643	0.996	0.002	0.999	0.984	Accepted	1.02E-04	0.024
MiF-1	− 0.367	0.01	0.137	0.009	0.83	Accepted	1.91E-05	0.032
Betanin-MiF-1	− 1.373	0.997	0.102	0	0.936	Accepted	1.14E-04	0.008
Betanin-di-MiF-1	− 1.148	0.996	0.089	0	0.881	Accepted	6.60E-05	0.008
Betanin-tri-MiF-1	− 0.193	0.999	0.056	0	0.881	Accepted	4.94E-05	0.008
Gallate-MiF-1	− 0.482	0.32	0.351	0.001	0.981	Accepted	3.30E-06	0.007
Pomolate-MiF-1	4.655	0.042	0.689	0.745	0	Accepted	2.97E-05	0.015
Sinapate-MiF-1	0.944	0.236	0.978	0.146	0.988	Accepted	5.65E-06	0.034

order to predict their potential effectiveness as drug candidates. This includes the absorption, distribution, metabolism, excretion properties of the conjugates [70]. The results are shown in Table 5. We compared the logP, blood brain barrier (BBB) penetration, PgP inhibitor/substrate status, Madin-Darby Canine Kidney cell (MDCK) permeability, human ether-a-go-go related gene (hERG) blocker potential, and intestinal absorption of each conjugate. LogP predicts the membrane permeability and lipophilicity of compounds, with an ideal range for drugs being between 0 and 3 log mol/L [71]. Pomolate-NPFF and pomolate-MiF-1 were found to have the highest logP values due to the presence of the pentacyclic terpene moiety. All other conjugates appeared to have fall within the desired logP value range of drug candidacy. NPFF and all its conjugates appear to fall within this range.

Since these conjugates are intended to interact with receptors widely present in the CNS, we also sought to predict Blood Brain Barrier (BBB) permeability. According to Admet2.0 lab, output values within the range of 0–0.3 are considered excellent for BBB permeability while those in the range of 0.3–0.7 are considered to display medium permeability. Additionally, drug candidates with values in the range of 0.7–1.0 are considered to have poor BBB permeability. Thus, all conjugates and peptides with the exception of sinapate-MiF-1 and pomolate-MiF-1 are predicted to be BBB permeable.

Next, we examined the potential of the conjugates to behave as either PgP inhibitor or substrates. P-glycoprotein (PgP) is a member of the ATP-binding cassette transporters and plays an important role in the efflux of a wide variety of drugs. Thus, PgP inhibitors can prolong the time the drug is present in the cell [72]. Values in the range of 0–0.7 are considered good inhibitors/substrates while output values above 0.7 are considered poor PgP inhibitors/substrates. Based on those parameters, NPFF and pomolate-MiF-1 are poor PgP inhibitors while all other conjugates fall within the functional range of PgP inhibitors. NPFF, betanin-NPFF, betanin-di-NPFF, betanin-tri-NPFF, pomolate-NPFF and pomolate-MiF-1 were found to be substrates for PgP, while all other conjugates were predicted to be poor substrates. This implies that most of the MiF-1 conjugates may be predicted to have better absorption.

The Pfizer rule [73] predicts that compounds with a logP greater than 3 and a topological polar surface area less than 75 are likely to have less drug likelihood and may be toxic. All of the conjugates, and the peptides were found have logP values less than three with the exception of the pomolate conjugates due to its hydrophobicity, thus most of the designed conjugates were accepted by the Pfizer rule. MDCK permeability allows for determining drug uptake by cells which can be used to determine the efficacy of drugs [74]. In general, values of Papp $> 2 \times 10^{-6}$ cm/s are predicted to exhibit MDCK permeability. Our results showed that all conjugates were predicted to be permeable except sinapate-MiF-1 which had a slightly higher range of 5.65E-06.

We next determined whether the conjugates were likely to be hERG blockers, which would impact cardiac muscle depolarization resulting in severe heart issues and can be harmful. The hERG blocker potential of the conjugates was determined on a probability scale, with scores near 1.0 being considered to have a high probability of being a hERG blocker [75]. All of the conjugates studied scored very low on this scale, indicating that none of the conjugates are predicted to be hERG blockers.

Table 6 KD* values obtained for each of the conjugates upon binding to the NOP receptor

Peptide/Conjugate	KD (μM)
Pomolate-MiF-1	72 ± 3.4
Betanin-Tri-MiF-1	25.1 ± 4.7
Sinapate-MiF-1	Could not be determined
Gallate-MiF-1	41 ± 2.1
MiF-1	98.5 ± 3.2
Pomolate-NPFF	39.2 ± 5.3
Betanin-Tri-NPFF	17.3 ± 4.0
Sinapate-NPFF	32.4 + 2.1
Gallate-NPFF	49 ± 4.2
NPFF	22.5 ± 3.6

* Values reported are averages of three separate runs

SPR analysis

As a proof of concept, in order to examine the binding interactions with the optimal conjugates, we conducted SPR analysis of the peptides and the corresponding conjugates with NOP/ORL1 Opioid Receptor Membranes with high levels of OPRL1 surface expression, which are utilized to determine ligand binding elucidate effects of NOP receptor ligands. In the case of the betanin conjugates, we evaluated the binding interactions with the tri-peptide conjugates, as those showed stable binding in the computational studies. All others were monoconjugates that were designed and synthesized as described earlier. For SPR analysis, the gold surface of the sensor chip is functionalized in order to attach the NOPR as explained in the methods section. Each analyte (conjugate or peptide) was then injected into the system and binding interactions over time were probed [76]. The sensograms obtained at varying concentrations of each

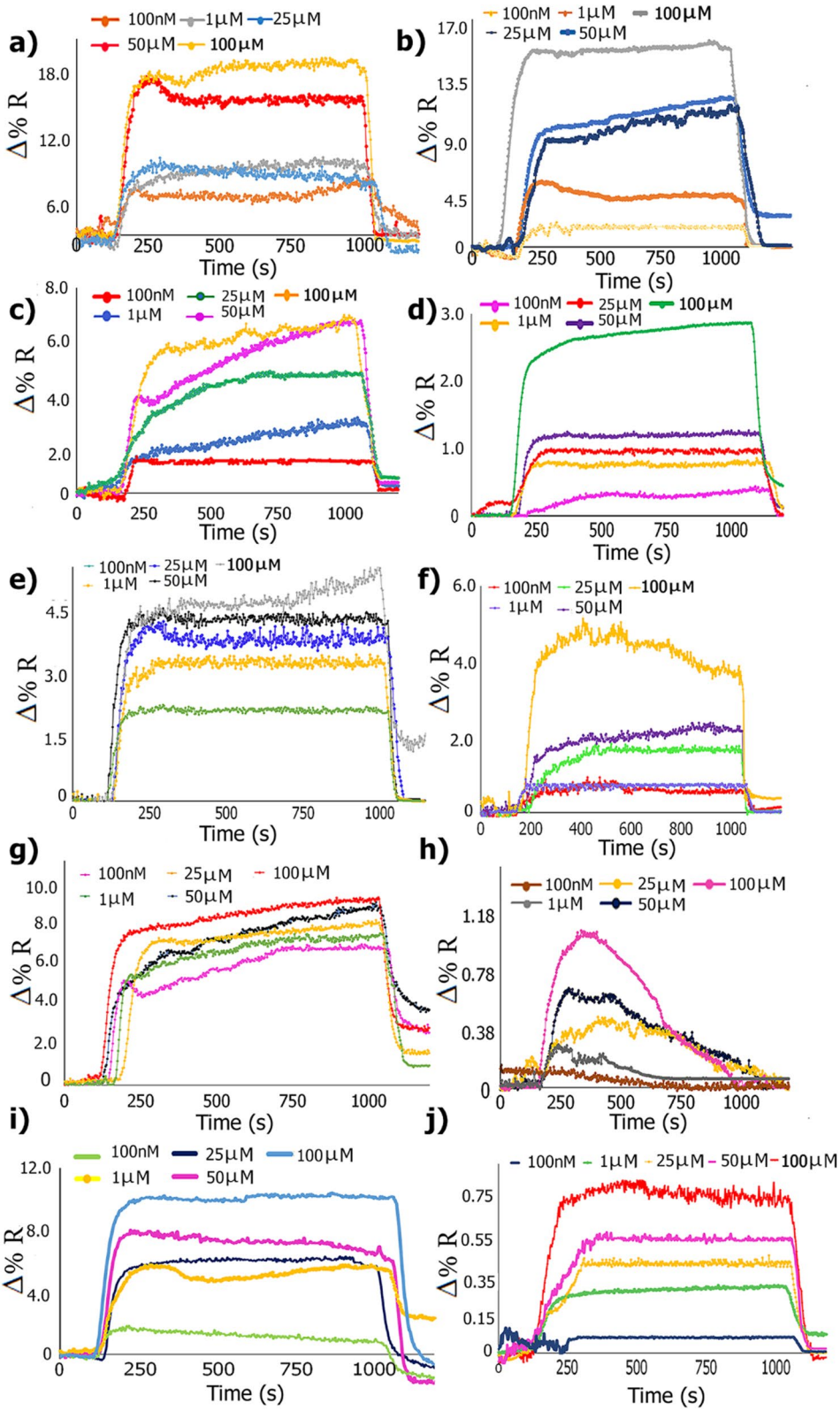

Fig. 9 SPR sensograms showing percent change in reflectivity over time. The NOPR receptor was immobilized on to gold chips and each analyte was run for an average of 1200 s. Values reported are averages of three separate runs (**a**) Betanin-Tri-NPFF; (**b**) Betanin-Tri-MiF1; (**c**) Pomolate-NPFF; (**d**) Pomolate-MiF1; (**e**) Gallate-NPFF; (**f**) Gallate-MiF1; (**g**) Sinapate-NPFF; (**h**) Sinapate-MiF1; (**i**) NPFF; (**j**) MiF1

of the ligands are shown in Fig. 9. The corresponding KD values were obtained using non-linear regression analysis using GraphPad software are shown in Table 6. Among the NPFF candidates, the highest binding was seen for betanin-tri-NPFF and sinapate-NPFF, while the neat peptide NPFF showed slightly lesser binding compared to those conjugates. The pomolate-NPFF showed intermediate binding comparably, while the lowest binding was observed for gallate-NPFF conjugates. These results corroborate with the computational analysis where it was shown that among the NPFF conjugates, the betanin-conjugates showed highest binding.

Overall, MiF-1 conjugates showed relatively lower binding compared to the NPFF conjugates. The betanin-tri-MiF-1 conjugate was the only conjugate to show relatively high binding with the receptor, followed by gallate-MiF-1 and pomolate-MiF-1. The neat peptide showed significantly slower and lesser binding. The KD for sinapate-MiF-1 could not be determined because binding was minimal at lower concentrations and at higher concentrations; while we did observe association, the conjugate showed rapid detachment within 300 s, indicating overall poor binding. Thus, sinapate-MiF1 demonstrated poor binding interactions with the NOPR. Once again, these results corroborate with the computational studies which showed weakest binding with the sinapate-MiF-1 conjugate. The weak binding for the sinapate-MiF-1 could be attributed to the fact that this conjugate fails to attach to the binding pocket. It is likely that the conjugate is unstable in that region and quickly detaches. Overall, in both cases, the betanin tri-conjugates demonstrated the most optimal binding, and the NPFF conjugates in general showed relatively higher binding. Thus, it appears that the NPFF peptide has more favorable interactions with the receptor and that coupled with the structures of the phytochemicals enhances binding with the binding pocket, as was demonstrated in the computational studies.

Phytochemical conjugates of two known neuropeptides MiF-1 and NPFF with pain modulating ability were developed. The binding interactions of those conjugates with NOP receptor was examined as a strategy to develop novel natural peptide-based drug candidates that can potentially modulate NOP receptor activity. Each of the phytochemicals selected are antioxidants which may play a role in mitigating neurodegenerative diseases. Our results indicated that the betanin conjugates with both peptides showed strong binding interactions in addition to gallate MiF-1, gallate-NPFF and sinapate-NPFF while the pomolate-NPFF conjugate showed moderate binding. Docking and molecular dynamics studies revealed that binding interactions occurred at the binding pocket encompassing the transmembrane helices TM1, TM3 and TM7 in most cases, with the ligands binding deep within the hydrophobic core. The binding interactions were further confirmed experimentally through SPR analysis, which once again showed high binding with the betanin conjugates. MMGBSA analysis revealed that the binding energies were enhanced in all cases when MiF-1 was conjugated to the phytochemicals compared to neat MiF-1. However, in the case of NPFF, while the betanin conjugates showed enhancement, in some cases the binding energies were found to be slightly reduced compared to neat NPFF, which in itself showed strong binding. ADME prediction studies revealed the conjugates are likely to be MDCK cell permeable, and were not hERG blockers. Overall our studies reveal that such natural phytochemical derivatives can bind to the NOP receptor when conjugated to the mammalian amidated neuropeptide NPFF and the short sequence of melanocyte inhibiting fact MiF-1 and may be developed for further laboratory studies for potential pharmaceutical applications.

Supplementary Information

The online version contains supplementary material available at https://doi.org/10.1186/s13765-024-00876-9.

Additional file 1: Figure S1. Sigma Profile and Sigma Surface obtained for the endogenous ligand FGGFTGARKSARKLANQ. Red =H-bond acceptor region, Blue = H-bond donor region and Green = Non-polar region. **Table S2.** PLIP interactions showing receptor residues involved in binding with each of the peptides and conjugates. **Figure S2.** Protein-ligand contacts for NOPR with NPFF and its conjugates (a) NPFF; (b) Gallate-NPFF; (c) Pomolate-NPFF; (d) Sinapate-NPFF; (e) Betanin-NPFF; (f) Betanin-di-NPFF; (g) Betanin-tri-NPFF. **Figure S3.** Protein-ligand contacts of NOPR with MiF-1 and conjugates. (a) MiF-1; (b) Gallate-MiF-1; (c) Pomolite-MiF-1; (d) Sinapate-MiF-1; (e) Betanin-MiF-1; (f) Betanin-di-MiF-1; (g) Betanin-tri-MiF-1. **Figure S4.** (a) Trajectory analysis of FGGFTGARKSARKLANQover 100 ns simulation. Images are shown at 0ns, 50 ns and at 100 ns. (b) Radius of gyration of the FGGFTGARKSARKLANQwhen complexed with the NOPR over 100 ns simulation; (c) Plot of RMSF for the protein back bone when complexed with FGGFTGARKSARKLANQ.

Acknowledgements

The authors thank the Advanced Research Computing, Education Technologies and Research Computing Department at Fordham University, a division of the Office of Information Technology for providing their assistance and access to research computing resources that have contributed to the computational results reported here.

Author contributions

Conception, writing, and design of study: IAB; Acquisition of data: MEM, BGG, MAB and SF and CGL. Analysis and interpretation of data: IAB and MEM. MEM was also involved in writing the initial drafts of the manuscript. IAB wrote and edited the final manuscript.

Funding

The authors thank Fordham University Research Grants for financial support of this work. MM, BG and MB thank the Henry Luce Foundation for the Clare Boothe Luce Scholarship for funding.

Availability of data and materials
Associated data are included in the Additional file 1. The manuscript will be shared on faculty website.

Code availability
Not applicable.

Declarations

Ethics approval and consent to participate
Not applicable.

Consent for publication
Not applicable.

Competing interests
The authors declare no competing interests.

Author details
[1]Department of Chemistry and Biochemistry, Fordham University, 441 East Fordham Road, Bronx, NY 10458, USA.

Received: 3 June 2023 Accepted: 15 February 2024
Published online: 09 March 2024

References

1. Filizola M, Devi LA (2013) Grand opening of structure-guided design for novel opioids. Trends Pharmacol Sci 34(1):6–12. https://doi.org/10.1016/j.tips.2012.10.002
2. McDonald J, Lambert DG (2015) Opioid receptors. BJA Educ 15:219–224. https://doi.org/10.1093/bjaceaccp/mku041
3. Toll L, Cippitelli A, Ozawa A (2021) The NOP receptor system in neurological and psychiatric disorders: discrepancies, peculiarities and clinical progress in developing targeted therapies. CNS Drugs 35(6):591–607. https://doi.org/10.1007/s40263-021-00821-0
4. Shimohigashi Y, Hatano R, Fujita T, Nakashima R, Nose T, Sujaku T, Saigo A, Shinjo K, Nagahisa A (1996) Sensitivity of opioid receptor-like receptor ORL1 for chemical modification on nociceptin, a naturally occurring nociceptive peptide. J Biol Chem 271(39):23642–23645. https://doi.org/10.1074/jbc.271.39.23642
5. Neal CR Jr, Mansour A, Reinscheid R, Nothacker HP, Civelli O, Akil H, Watson SJ Jr (1999) Opioid receptor-like (ORL1) receptor distribution in the rat central nervous system: comparison of ORL1 receptor mRNA expression with 125I-[14Tyr]-orphanin FQ binding. J Comp Neurol 412(4):563–605. https://doi.org/10.1002/(SICI)1096-9861(19991004)412:4%3c563::AID-CNE2%3e3.0.CO;2-Z
6. Mercatelli D, Bezard E, Eleopra R, Zaveri NT, Morari M (2020) Managing Parkinson's disease: moving ON with NOP. Br J Pharmacol 177(1):28–47. https://doi.org/10.1111/bph.14893
7. Hernandez J, Fabelo C, Perez L, Moore C, Chang R, Wagner EJ (2019) Nociceptin/orphanin FQ modulates energy homeostasis through inhibition of neurotransmission at VMN SF-1/ARC POMC synapses in a sex-and diet-dependent manner. Biol Sex Differ 10:1–24. https://doi.org/10.1186/s13293-019-0220-3
8. Zaveri NT (2016) Nociceptin opioid receptor (NOP) as a therapeutic target: progress in translation from preclinical research to clinical utility: miniperspective. J Med Chem 59(15):7011–7028. https://doi.org/10.1021/acs.jmedchem.5b01499
9. Kiguchi N, Ding H, Ko MC (2016) Central N/OFQ-NOP receptor system in pain modulation. Adv Pharmacol 75:217–243. https://doi.org/10.1016/bs.apha.2015.10.001
10. Du LN, Wu GC, Cao XD (1998) Modulation of orphanin FQ or electroacupuncture (EA) on immune function of traumatic rats. Acupunc Electrother Res 23(1):1–8. https://doi.org/10.3727/036012998816356580
11. Norton CS, Neal CR, Kumar S, Akil H, Watson SJ (2002) Nociceptin/orphanin FQ and opioid receptor-like receptor mRNA expression in dopamine systems. J Comp Neurol 444(4):358–368. https://doi.org/10.1002/cne.10154
12. Marti M, Sarubbo S, Latini F, Cavallo M, Eleopra R, Biguzzi S, Lettieri C, Conti C, Simonato M, Zucchini S, Morari M (2010) Brain interstitial nociceptin/orphanin FQ levels are elevated in Parkinson's disease. Mov Disord 25(11):1723–1732. https://doi.org/10.1002/mds.23271
13. Jia YP, Linden DR, Serie JR, Seybold VS (1998) Nociceptin/orphanin FQ binding increases in superficial laminae of the rat spinal cord during persistent peripheral inflammation. Neurosci Lett 250(1):21–24. https://doi.org/10.1016/S0304-3940(98)00430-3
14. Borruto AM, Fotio Y, Stopponi S, Petrella M, De Carlo S, Domi A, Ubaldi M, Weiss F, Ciccocioppo R (2021) NOP receptor antagonism attenuates reinstatement of alcohol-seeking through modulation of the mesolimbic circuitry in male and female alcohol-preferring rats. Neuropsychopharmacol 46(12):2121–2131. https://doi.org/10.1038/s41386-021-01096-1
15 Post A, Smart TS, Krikke-Workel J, Dawson GR, Harmer CJ, Browning M, Witkin JM (2016) A selective nociceptin receptor antagonist to treat depression: evidence from preclinical and clinical studies. Neuropsychopharmacology 41(7):1803–1812. https://doi.org/10.1038/npp.2015.348
16. Marti M, Trapella C, Viaro R, Morari M (2007) The nociceptin/orphanin FQ receptor antagonist J-113397 and L-DOPA additively attenuate experimental parkinsonism through over inhibition of the nigrothalamic pathway. J Neurosci 27(6):1297–1307. https://doi.org/10.1523/JNEUROSCI.4346-06.2007
17. N T (2011) The nociception/orphanin FQ receptor (NOP) as a target for drug abuse. Curr Top Med Chem 11(9):1151–1156. https://doi.org/10.2174/156802611795371341
18. DeWire SM, Yamashita DS, Rominger DH, Liu G, Cowan CL, Graczyk TM, Chen X, Pitis PM, Gotchev D, Yuan C, Koblish M, Lark MW, Violin JD (2013) A G protein-biased ligand at the μ-opioid receptor is potently analgesic with reduced gastrointestinal and respiratory dysfunction compared with morphine. J Pharmacol Exp Ther 344(3):708–717. https://doi.org/10.1124/jpet.112.201616
19. Spetea M, Eans SO, Ganno ML, Lantero A, Mairegger M, Toll L, Schmidhammer H, McLaughlin JP (2017) Selective κ receptor partial agonist HS666 produces potent antinociception without inducing aversion after icv administration in mice. Br J Pharmacol 174(15):2444–2456. https://doi.org/10.1111/bph.13854
20. Daga PR, Zaveri NT (2012) Homology modeling and molecular dynamics simulations of the active state of the nociceptin receptor reveal new insights into agonist binding and activation. Proteins Struct Funct Bioinf 80(8):1948–1961. https://doi.org/10.1002/prot.24077
21. Bröer BM, Gurrath M, Höltje HD (2003) Molecular modelling studies on the ORL1-receptor and ORL1-agonists. J Comput Aided Mol Des 17:739–754. https://doi.org/10.1023/B:JCAM.0000017491.97244.69
22. Liu M, He L, Hu X, Liu P, Luo HB (2010) 3D-QSAR, homology modeling, and molecular docking studies on spiropiperidines analogues as agonists of nociceptin/orphanin FQ receptor. Bioorg Med Chem Lett 20(23):7004–7010. https://doi.org/10.1016/j.bmcl.2010.09.116
23. Dickinson SL, Slater P (1980) Opiate receptor antagonism by L-prolyl-L-leucyl-glycinamide. MIF-I Peptides 1(4):293–299. https://doi.org/10.1016/0196-9781(80)90006-6
24. Pan W, Kastin AJ (2007) From MIF-1 to endomorphin: the Tyr-MIF-1 family of peptides. Peptides 28(12):2411–2434. https://doi.org/10.1016/j.peptides.2007.10.006
25. Moulédous L, Mollereau C, Zajac JM (2010) Opioid-modulating properties of the neuropeptide FF system. BioFactors 36(6):423–429. https://doi.org/10.1002/biof.116
26. Kujawska M, Jodynis-Liebert J (2018) Polyphenols in Parkinson's disease: a systematic review of in vivo studies. Nutrients 10(5):642. https://doi.org/10.3390/nu10050642
27. Katavic PL, Lamb K, Navarro H, Prisinzano TE (2007) Flavonoids as opioid receptor ligands: identification and preliminary structure−activity relationships. J Nat Prod 70(8):1278–1282. https://doi.org/10.1021/np070194x
28. Subbannayya Y, Karthikkeyan G, Pinto SM, Kapoor S, Tyagi A, Pervaje SK, Pervaje R, Prasad TSK (2018) Global metabolite profiling and network pharmacology of triphala identifies neuromodulatory receptor proteins as potential targets. J Proteins Proteomics 9(2):101–114
29. Charoenchai L, Wang H, Wang JB, Aldrich JV (2008) High affinity conformationally constrained nociception/orphanin FQ (1–13) amide analogues. J Med Chem 51(15):4385–4387. https://doi.org/10.1021/jm800394v

30. Calo G, Rizzi A, Rizzi D, Bigoni R, Guerrini R, Marzola G, Marti M, McDonald J, Morari M, Lambert DG, Salvadori S, Regoli D (2002) [Nphe1, Arg14, Lys15] nociceptin-NH2, a novel potent and selective antagonist of the nociceptin/orphanin FQ receptor. Br J Pharmacol 136:303–311. https://doi.org/10.1038/sj.bjp.0704706
31. Okada K, Sujaku T, Chuman Y, Nakashima R, Nose T, Costa T, Yamada Y, Yokoyama M, Nagahisa A, Shimohigashi Y (2000) Highly potent nociceptin analog containing the Arg-Lys triple repeat. Biochem Biophys Res Commun 278:493–498. https://doi.org/10.1006/bbrc.2000.3822
32. Zhang C, Miller W, Valenzano KJ, Kyle DJ (2002) Novel, potent ORL-1 receptor agonist peptides containing alpha-Helix-promoting conformational constraints. J Med Chem 45(24):5280–5286. https://doi.org/10.1021/jm0202021
33 Guerrini R, Marzola E, Trapella C, Pela' M, Molinari S, Cerlesi MC, Malfacini D, Rizzi A, Salvadori S, Calo' G (2014) A novel and facile synthesis of tetra branched derivatives of nociceptin/orphanin FQ. Bioorg Med Chem 22(14):3703–3712. https://doi.org/10.1016/j.bmc.2014.05.005
34. Lohman R-J, Harrison RS, Ruize-Gomez G, Hoang HN, Shepherd NE, Chow S, Hill TA, Madala P, Fairlie DP (2015) Helix-constrained nociceptin peptides are potent agonists and antagonists of ORL-1 and nociception. Vitam Horm 97:1–55. https://doi.org/10.1016/bs.vh.2014.10.001
35. Al-Hasani R, Bruchas MR (2011) Molecular mechanisms of opioid receptor-dependent signaling and behavior. Anesthesiology 115(6):1363–1381. https://doi.org/10.1097/ALN.0b013e318238bba6
36. Donica CL, Awwad HO, Thakker DR, Standifer KM (2013) Cellular mechanisms of nociceptin/orphanin FQ (N/OFQ) peptide (NOP) receptor regulation and heterologous regulation by N/OFQ. Mol Pharmacol 83(5):907–918. https://doi.org/10.1124/mol.112.084632
37. Meunier JC, Mollereau C, Toll L, Suaudeau C, Moisand C, Alvinerie P, Butour JL, Guillemot JC, Ferrara P, Monsarrat B, Mazarguil H, Vassart G, Parmentier M, Costentin J (1995) Isolation and structure of the endogenous agonist of opioid receptor-like ORL1 receptor. Nature 377:532–535. https://doi.org/10.1038/377532a0
38 Toll L, Bruchas MR, Calo G, Cox BM, Zaveri NT (2016) Nociceptin/orphanin FQ receptor structure, signaling, ligands, functions, and interactions with opioid systems. Pharmacol Rev 68(2):419–457. https://doi.org/10.1124/pr.114.009209
39. Kwankaew N, Okuda H, Aye-Mon A, Ishikawa T, Hori K, Sonthi P, Kosakai Y, Ozaki N (2021) Antihypersensitivity effect of betanin (red beetroot extract) via modulation of microglial activation in a mouse model of neuropathic pain. Eur J Pain 25(8):1788–1803. https://doi.org/10.1002/ejp.1790
40. Kaur S, Muthuraman A (2019) Ameliorative effect of gallic acid in paclitaxel-induced neuropathic pain in mice. Toxicol Rep 6:505–513. https://doi.org/10.1016/j.toxrep.2019.06.001
41. Dzoyem JP, Nganteng DND, Melong R, Wafo P, Ngadjui B, Allemann E, Delie F (2021) Bioguided identification of pentacyclic triterpenoids as anti-inflammatory bioactive constituents of Ocimum gratissum extract. J Ethnopharmacol 268:113637. https://doi.org/10.1016/j.jep.2020.113637
42. Chen C (2016) Sinapic acid and its derivatives as medicine in oxidative stress-induced diseases and aging. Oxid Med Cell Longevity 2016:357614. https://doi.org/10.1155/2016/3571614
43. Alaofi AL (2020) Sinapic acid ameliorates the progression of streptozotocin (STZ)-induced diabetic nephropathy in rats *via* NRF2/HO-1 mediated pathways. Front Pharmacol 11:1119. https://doi.org/10.3389/fphar.2020.01119
44. Mustazza C, Borioni A, Sestili I, Sbraccia M, Rodomonte A, Del Giudice MR (2008) Synthesis and pharmacological evaluation of 1,2-dihydrospiro[isoquinoline-4(3H),4′-piperidin]-3-ones as nociceptin receptor agonists. J Med Chem 51(4):1058–1062. https://doi.org/10.1021/jm7009606
45. Caldwell JP, Matasi JJ, Fernandez X, McLeod RL, Zhang H, Fawzi A, Tulshian Deen B (2009) Synthesis and structure-activity relationships of N-substituted spiropiperidines as nociceptin receptor ligands: part 2. Bioorg Med Chem Lett 19(4):1164–1167. https://doi.org/10.1016/j.bmcl.2008.12.092
46. Ho GD, Anthes J, Bercovici A, Caldwell JP, Cheng KC, Cui X, Fawzi A, Fernandez X, Greenlee WJ, Hey J, Korfmacher W, Lu SX, McLeod RL, Ng F, Torhan AS, Tan Z, Tulshian D, Varty GB, Xu X, Zhang H (2009) The discovery of tropane derivatives as nociceptin receptor ligands for the management of cough and anxiety. Bioorg Med Chem Lett 19(9):2519–2523. https://doi.org/10.1016/j.bmcl.2009.03.031
47. COSMOtherm, version C3.0, Release 19, COSMO logic GmbH and Co. KG: Leverkusen, Germany, 2019
48. Mullins E, Oldland R, Liu YA, Wang S, Sandler SI, Chen CC, Zwolak M, Seavey KC (2006) Sigma-profile database for using COSMO-based thermodynamic methods. Ind Eng Chem Res 45(12):4389–4415. https://doi.org/10.1021/ie060370h
49. Gonzalez-Miquel M, Massel M, DeSilva A, Palomar J, Rodriguez F, Brennecke JF (2014) Excess enthalpy of monoethanolamine+ ionic liquid mixtures: how good are COSMO-RS predictions? J Phys Chem B 118(39):11512–11522. https://doi.org/10.1021/jp507547q
50. Thompson AA, Liu W, Katritch V, Wu H, Vardy E, Huang X-P, Trapella C, Guerrini R, Calo G, Roth BL, Cherezov V, Stevens RC (2012) Structure of nociception/orphanin FQ receptor in complex with peptide mimetic. Nature 485:395–399. https://doi.org/10.1038/nature11085
51. Yu J, Zhou Y, Tanaka I, Yao M (2010) Roll: a new algorithm for the detection of protein pockets and cavities with a rolling probe sphere. Bioinformatics 26(1):46–52. https://doi.org/10.1093/bioinformatics/btp599
52. Trott O, Olson AJ (2010) AutoDock Vina: improving the speed and accuracy of docking with a new scoring function, efficient optimization, and multithreading. J Comput Chem 31(2):455–461. https://doi.org/10.1002/jcc.21334
53. The PyMOL Molecular Graphics System, Version 2.0 Schrödinger, LLC.
54. Adasme MF, Linnemann KL, Bolz SN, Kaiser F, Salentin S, Haupt VJ, Schroeder M (2021) PLIP 2021: expanding the scope of the protein–ligand interaction profiler to DNA and RNA. Nucleic Acids Res 49(W1):W530–W534. https://doi.org/10.1093/nar/gkab294
55. Bowers KJ, Chow E, Xu H, Dror RO, Eastwood MP, Gregersen BA, Klepeis J, Kolossvary I, Moraes MA, Sacerdoti FD, Salmon JK, Shan Y, Shaw DE. (2006). Scalable algorithms for molecular dynamics simulations on commodity clusters. In SC'06: Proceedings of the 2006 ACM/IEEE Conference on Supercomputing (pp. 84-es). https://doi.org/10.1145/1188455.1188544
56. Venugopal PP, Das BK, Soorya E, Chakraborty D (2020) Effect of hydrophobic and hydrogen bonding interactions on the potency of ß-alanine analogs of G-protein coupled glucagon receptor inhibitors. Proteins Struct Funct Bioinf 88(2):327–344. https://doi.org/10.1002/prot.25807
57. Du J, Sun H, Xi L, Li J, Yang Y, Liu H, Yao X (2011) Molecular modeling study of checkpoint kinase 1 inhibitors by multiple docking strategies and prime/MM–GBSA calculation. J Comput Chem 32(13):2800–2809. https://doi.org/10.1002/jcc.21859
58 Hou T, Wang J, Li Y, Wang W (2011) Assessing the performance of the MM/PBSA and MM/GBSA methods. 1. The accuracy of binding free energy calculations based on molecular dynamics simulations. J Chem Inf Model 51(1):69–82. https://doi.org/10.1021/ci100275a
59 Xiong G, Wu Z, Yi J, Fu L, Yang Z, Hsieh C, Cao D (2021) ADMETlab 2.0: an integrated online platform for accurate and comprehensive predictions of ADMET properties. Nucleic Acids Res 49(W1):W5–W14. https://doi.org/10.1093/nar/gkab255
60. Fischer MJE (2010) Amine coupling through EDC/NHS: a practical approach. Methods Mol Biol 627:55–73. https://doi.org/10.1007/978-1-60761-670-2_3
61. Bourassa P, Tudashki HB, Pineyro G, Grandbois M, Gendron L (2014) Label-free monitoring of μ-opioid receptor-mediated signaling. Mol Pharmacol 86(2):138–149. https://doi.org/10.1124/mol.114.093450
62. Mullins E, Liu YA, Ghaderi A, Fast SD (2008) Sigma profile database for predicting solid solubility in pure and mixed solvent mixtures for organic pharmacological compounds with COSMO-based thermodynamic methods. Ind Eng Chem Res 47(5):1707–1725. https://doi.org/10.1021/ie0711022
63. Lemaoui T, Darwish AS, Hammoudi NEH, Abu Hatab F, Attoui A, Alnashef IM, Benguerba Y (2020) Prediction of electrical conductivity of deep eutectic solvents using COSMO-RS sigma profiles as molecular descriptors: a quantitative structure–property relationship study. Ind Eng Chem Res 59(29):13343–13354. https://doi.org/10.1021/acs.iecr.0c02542
64 Della Longa S, Arcovito A (2016) A dynamic picture of the early events in nociceptin binding to the NOP receptor by metadynamics. Biophys J 111(6):1203–1213. https://doi.org/10.1016/j.bpj.2016.07.004

65. Della Longa S, Arcovito A (2018) In silico study of the binding of two novel antagonists to the nociceptin receptor. J Comput-Aided Mol Des 32:385–400. https://doi.org/10.1007/s10822-017-0095-5
66. Della LS, Arcovito A (2019) Microswitches for the activation of the nociceptin receptor induced by cebranopadol: hints from microsecond molecular dynamics. J Chem Inf Model 59:818–831. https://doi.org/10.1021/acs.jcim.8b00759
67. Shoblock JR (2007) The pharmacology of Ro 64–6198, a systemically active, nonpeptide NOP receptor (opiate receptor like 1, ORL-1) agonist with diverse preclinical therapeutic activity. CNS Drug Rev 13(1):107–136. https://doi.org/10.1111/j.1527-3458.2007.00007.x
68. Kothandan G, Gadhe CG, Balupuri A, Ganapathy J, Cho SJ (2014) The nociceptin receptor (NOPR) and its interaction with clinically important agonist molecules: a membrane molecular dynamics simulation study. Mol bioSystems 10(12):3188–3198
69. Wang E, Sun H, Wang J, Wang Z, Liu H, Zhang J, Hou T (2019) End-point binding free energy calculation with MM/PBSA and MM/GBSA: strategies and applications in drug design. Chem Rev 119:9478–9508. https://doi.org/10.1021/acs.chemrev.9b00055
70. Ratain Mark J, Plunkett WK Jr (2003) Principles of pharmacokinetics. In: Kufe DW, Pollock RE, Weicheselbaum RR et al (eds) Holland-Frei cancer medicine, 6th edn. BC Decker, Hamilton
71 Shin HK, Kang Y-M, No KT (2017) Predicting ADME properties of chemicals. In: Leszczynski J, Kaczmarek-Kedziera A, Puzyn T, Papadopoulos MG, Reis H, Shukla MK (eds) Handbook of computational chemistry. Springer, Cham
72. Lin JH, Yamazaki M (2003) Role of P-glycoprotein in pharmacokinetics. Clin Pharmacokinet 42(1):59–98. https://doi.org/10.2165/00003088-200342010-00003
73. Yukawa T, Naven R (2020) Utility of physicochemical properties for the prediction of toxicological outcomes: takeda perspective. ACS Med Chem Lett 11:203–209. https://doi.org/10.1021/acsmedchemlett.9b00536
74. Williams J, Siramshetty V, Nguyen D-T, Padiha EC, Kabir M, Yu K-R, Wang AQ, Zhao T, Itkin M, Shinn P, Mathe EA, Xu X, Shah, (2022) Using in vitro ADME data for lead compound selection: an emphasis on PAMPA pH 5 permeability and oral bioavailability. P Bioorg Med Chem 56:116588. https://doi.org/10.1016/j.bmc.2021.116588
75. Sun H, Huang R, Xia M, Shahane S, Southall N, Wang Y (2017) Prediction of hERG liability–using SVM classification, bootstrapping and jackknifing. Mol Inform. https://doi.org/10.1002/minf.201600126
76. Stahelin RV (2013) Surface plasmon resonance: a useful technique for cell biologists to characterize biomolecular interactions. Mol Biol Cell 24(7):883–886. https://doi.org/10.1091/mbc.E12-10-0713

Publisher's Note